The transition on North America from the warm humid Pliocene to the glaciated Quaternary traced by eolian dust deposition at a benchmark North Atlantic Ocean drill site

David C. Lang[1], Ian Bailey[1,2]*, Paul A. Wilson[1], Christopher J. Beer[1], Clara T. Bolton[1,3], Oliver Friedrich[1,4], Cherry Newsam[1,5], Megan R. Spencer[1], Marcus Gutjahr[1,6], Gavin L. Foster[1], Matthew J. Cooper[1], J. Andrew Milton[1]

1. National Oceanography Centre Southampton, University of Southampton, Waterfront Campus, European Way, Southampton SO14 3ZH, UK.

2. Present address: Camborne School of Mines, College of Engineering, Mathematics & Physical Sciences, University of Exeter, Penryn Campus, Treliever Road, Penryn, Cornwall TR10 9FE, UK.

3. Present address: Facultad de Geología, Universidad de Oviedo, Campus de Llamaquique, Jesús Arias de Velasco s/n, 33005 Oviedo, Spain.

4. Present address: Institute of Earth Sciences, University of Heidelberg, Im Neuenheimer Feld 234-236, 69120 Heidelberg, Germany

5. Present address: Earth Sciences, University College London, Gower Street, London WC1E 6BT, UK.

6. Present address: GEOMAR Helmholtz Centre for Ocean Research Kiel, Wischhofstrasse 1-3, 24148 Kiel, Germany

*Corresponding author (email: I.Bailey@exeter.ac.uk)

Abstract

We present Plio-Pleistocene records of sediment color, %$CaCO_3$, foraminifer fragmentation, benthic carbon isotopes ($\delta^{13}C$) and radiogenic isotopes (Sr, Nd, Pb) of the terrigenous component from IODP Site U1313, a reoccupation of benchmark subtropical North Atlantic Ocean DSDP Site 607. We show that (inter)glacial cycles in sediment color and %$CaCO_3$ pre-date major northern hemisphere glaciation and are

unambiguously and consistently correlated to benthic oxygen isotopes back to 3.3 million years ago (Ma) and intermittently so probably back to the Miocene/Pliocene boundary. We show these lithological cycles to be driven by enhanced glacial fluxes of terrigenous material (aeolian dust), not carbonate dissolution (the classic interpretation). Our radiogenic isotope data indicate a North American source for this dust (~3.3 to 2.4 Ma) in keeping with the interpreted source of terrestrial plant wax-derived biomarkers deposited at Site U1313. Yet our data indicate a mid latitude provenance regardless of (inter)glacial state, a finding that is inconsistent with the biomarker-inferred importance of glaciogenic mechanisms of dust production and transport. Moreover, we find that the relation between biomarker and the lithogenic component of dust accumulation is distinctly non-linear. Both records show a jump in glacial rates of accumulation from MIS G6 (2.72 Ma) onwards but the amplitude of this signal is about 3 to 8 times greater for biomarkers than for dust and particularly extreme during MIS 100 (2.52 Ma). We conclude that North America shifted abruptly to a distinctly more arid and windy glacial regime from MIS G6, but major shifts in glacial North American vegetation biomes and regional wind fields (exacerbated by the growth of a large Laurentide ice sheet during MIS 100) likely explain amplification of this signal in the biomarker records. Our findings are consistent with wetter-than-modern reconstructions of North American continental climate under the warm high CO_2 conditions of the Early Pliocene but contrast with most model predictions for the response of the hydrological cycle to anthropogenic warming over the coming 50 years (poleward expansion of the subtropical dry zones).

Keywords: Pliocene; Quaternary; eolian; dust; North America, North Atlantic; Laurentide Ice Sheet.

1. Introduction

Deep-sea sediments in the climatically sensitive North Atlantic region are composed of two main constituents: biogenic carbonate ($CaCO_3$) produced in the overlying water column and allochtonous detrital material, with volcanic ash important only locally. It has long been recognised that striking rhythmic changes in the abundance of these constituents and therefore sediment color and $\%CaCO_3$ (Figure 1) provide both a high fidelity means of stratigraphic correlation and an expression of pronounced climate variability, especially in sediments deposited during times of significant northern hemisphere glaciation (NHG) (e.g. Ericson et al., 1961; Ruddiman and Glover, 1972).

Shackleton et al. (1984) drew attention to the remarkable correspondence between high amplitude changes in both benthic $\delta^{18}O$ and $\%CaCO_3$ back to earliest Pleistocene Marine Isotope Stage (MIS) 100 (2.52 Ma) at Deep Sea Drilling Project (DSDP) Site 552, where sediment deposition is dominated by pelagic rain from above. Prior to 2.52 Ma, variance in benthic $\delta^{18}O$ is unaccompanied by large amplitude change in $\%CaCO_3$ at Site 552 (Figure 1A). Originally, initiation of high-amplitude variance in color and $\%CaCO_3$ at this site was attributed by Shackleton et al. (1984) to onset of major NHG with $\%CaCO_3$ controlled by variations in the flux of non-carbonate material transported by ice rafting. We now know that the exact timing of the large decrease in $\%CaCO_3$ in sediments deposited at Site 552 is obscured because MIS G6 through 103 (2.72–2.58 Ma) fall in a core break (Raymo et al., 1989). As it happens, however, extensive work elsewhere shows MIS 100 to be the oldest glacial during which ice sheets were large enough (Ruddiman et al. 1987; Maslin et al. 1998; Jansen and Sjoholm, 1991; Jansen et al. 2000; Kleiven et al. 2002;

Bailey et al., 2013) and high latitude surface ocean temperatures cool enough (Lawrence et al. 2009; 2010; Naafs et al. 2010) to initiate ice-rafting on a basin-wide scale across the open North Atlantic Ocean.

In Figure 1A we show %$CaCO_3$ records from two further classic North Atlantic drill sites, DSDP 607 and 609 located on the southern fringe and at the centre of the last glacial IRD belt, respectively (Figure 2). Originally, %$CaCO_3$ variability at these two sites prior to ~2.5 Ma was attributed to sea floor $CaCO_3$ dissolution, a consequence of their greater water depth (Sites 609, ~3.9 km & 607, ~3.5 km, vs. 552 ~2.3 km, Figure 1A) and the influence of corrosive poorly ventilated southern-sourced bottom waters (Ruddiman et al., 1987; Ruddiman and Raymo, 1988). Yet, comparison of the %$CaCO_3$ plots compiled by Ruddiman et al. (1987) to records from shallower more recently drilled sites (Figure 1A vs. 1B) reveals that the timing of the initiation of marked lithological cycles in North Atlantic Ocean sediments is not a simple function of water depth indicating the influence of some factor other than $CaCO_3$ dissolution.

In principle, three mechanisms have the potential to deliver terrigenous sediments to Site U1313. But negligible Pliocene rates of accumulation of sand-sized IRD and volcanic grains at Integrated Ocean Drilling Program (IODP) Site U1313 (Bolton et al. 2010), the reoccupation of DSDP Site 607, confirms that the contemporaneous variability seen in %$CaCO_3$ (Figure 1) is not a function of melting icebergs over this classic site. Two alternative potential explanations must therefore be considered: (1) Transport beyond the contemporary iceberg front by ocean currents of fine-grained material delivered by ice-rafting to the Nordic Seas by the Greenland Ice Sheet (Winkler, 1999; Jansen et al., 2000; Andrews 2000). (2) Transport of continentally derived eolian dust from North Africa or from North America as inferred

103 based on biomarker records (Naafs et al., 2012).

104 To better understand the control(s) on, and climatic significance of, $\%CaCO_3$
105 variability of North Atlantic Ocean sediments deposited during the intensification of
106 northern hemisphere glaciation (iNHG) we present new orbital-resolution records of
107 carbonate dissolution, benthic $\delta^{13}C$, coarse lithic abundance and sediment $\%CaCO_3$
108 for IODP Site U1313, and radiogenic isotopes datasets that track the provenance of
109 terrigenous inputs to this site. We show that lithological cycles in North Atlantic
110 sediments of Pliocene age are driven by enhanced glacial fluxes of terrigenous
111 material, not carbonate dissolution. Our provenance work indicates that the
112 terrigenous component at the site is dominated by eolian dust sourced from the mid
113 latitudes of North America – a result consistent with published interpretations of the
114 record from Site U1313 of biomarkers derived from higher plant leaf waxes (Naafs et
115 al., 2012). A sharp increase in the biomarker proxy for dust inputs to our study site
116 during MIS G6, 2.72 Ma, is interpreted to reflect the importance of glacial grinding
117 by a large North American ice sheet complex in amplifying dust inputs to the North
118 Atlantic Ocean during glacials from this time (Naafs et al., 2012). Comparison among
119 data sets, however, indicates strong non-linearity in coupling between the dust and
120 biomarker records indicating that a reappraisal is merited of the sequence of climatic
121 events that they record and the mechanisms involved.
122

123 **2. Materials & Methods**

124 *2.1. IODP Site U1313*

125 IODP Site U1313 is located at the base of the upper western flank of the Mid Atlantic
126 Ridge at a water depth of 3426 m, ~240 nautical miles northwest of the Azores
127 archipelago (41°N, 32.5°W), on the extreme southerly limit of the last glacial "IRD

belt" (Ruddiman, 1977), a southwest-northeast trending band of maximum iceberg melting and hence IRD deposition between ~40°N and 55°N in the Atlantic Ocean (Figure 2). Site U1313 was drilled during IODP Expedition 306 and constitutes a reoccupation of DSDP Site 607, a benchmark mid-depth site monitoring North Atlantic Deep Water throughout the Plio-Pleistocene (Ruddiman et al., 1987; Raymo et al., 1989; Ruddiman et al., 1989; Raymo et al., 1992; Raymo et al., 2004). Site U1313 offers distinct advantages over its Site 607 precursor because it benefits from recovery by modern coring methods and from application of a full suite of physical property data collection and stratigraphic correlation techniques (Channel et al., 2010).

2.2. Stable isotope analysis, foraminifera fragmentation and chronology

Samples from IODP Site U1313 were obtained at 10 cm resolution from 114.12 to 155.28 meters composite depth (mcd) and washed over a 63 μm sieve. The ratio between fragments and whole foraminifera was established for the >150 μm fraction where more than 300 whole foraminifera were present following Ivanova et al. (2003). We focus our discussion on the interval 3.33 Ma (MIS MG1) to 2.41 Ma (MIS 95) covered by a published oxygen isotope stratigraphy (Bolton et al., 2010), measured on the benthic foraminifera *Cibicidoides wuellerstorfi* (>212 μm). For discussions of the younger Pleistocene portion of the Site U1313 record, we utilize the age model of Naafs et al. (2012) based on benthic $\delta^{18}O$ datasets spanning three time windows of the past 1 Myr (Stein et al., 2009; Feretti et al., 2010; Naafs et al., 2012) and shipboard correlation (Expedition 306 Scientists, 2006) of sediment physical properties (L*, lightness) to the LR04 stack (Lisiecki and Raymo, 2005). We present a new benthic $\delta^{13}C$ record from the samples analysed by Bolton et al. (2010) with an

external analytical precision, based on replicate analysis of an in-house standard calibrated to NBS-19, of ±0.031‰ (1σ).

2.3 Coarse lithic counts

The only high-resolution record of IRD deposition at Site U1313 for iNHG spans MIS 102-96 (Bolton et al., 2010). To improve our understanding of the history of IRD deposition at our study site during MIS M2 (3.3 Ma) and between MIS G6 and MIS 102 (2.72–2.56 Ma), new coarse lithic counts were performed on the >150μm size fraction between, respectively, 152.98–154.98 mcd and 120.74–129.86 mcd. The abundance of coarse lithics in Site U1313 sediments are very low throughout our study interval and are extremely low in sediments deposited prior to MIS 100 (2.52 Ma). To generate a statistically significant record of sand IRD abundance in Site U1313 sediments (expressed as IRD per gram of dry sediment) we therefore counted all coarse IRD (>150μm) in each sample studied.

2.4. Sediment color

There is a long history of attempts to develop rapid-throughput proxy methods to estimate sediment %$CaCO_3$ from the spectral properties of sediments (e.g. Chester and Elderfield, 1966). Use of optical lightness as an analytical tool in sediments recovered by DSDP and IODP has its roots in late Quaternary studies (Balsam, 1981), was pioneered by grey-scale analysis of photographs (e.g. Herbert and D'Hondt, 1990; Busch, 1991) and is now determined routinely from sediment color in sediments of appropriate lithology. Sediment color can be defined using three variables, a* (red-green), b* (blue-yellow) and L* (lightness), that lie along mutually perpendicular axes in color space. We obtained shipboard color reflectance data at 2

cm resolution for Site U1313 from the IODP database website (http://iodp.tamu.edu/database/index.html), generated using a modern version of the split core automatic track reflectance spectrometer first trialled to remarkable effect during Ocean Drilling Program (ODP) Leg 138 (Mix et al., 1992; Mix et al., 1995; Ortiz et al., 1999). Here we employ records of L* to represent sediment color.

A comparison of L* data for Site U1313 and discrete $\%CaCO_3$ measurements generated post-cruise on sediments deposited during MIS 16–9 (640–320 ka; Stein et al., 2009) illustrates that large variations in L* for Site U1313 sediments deposited over late Pleistocene glacial-interglacial cycles correspond to pronounced variations (of ~30 %) in sediment $\%CaCO_3$ (Figure 3). To improve our understanding of the relationship between sediment color and $\%CaCO_3$ for the Pliocene portion of the Site U1313 record (for which L* values are typically higher and amplitude change muted relative to those documented for the Pleistocene) we generated 193 new $\%CaCO_3$ estimates on small (~0.5 cc), discrete samples using a standard (LECO) combustion technique following Stein et al. (2009).

To generate a high-resolution record of $\%CaCO_3$ of Site U1313 sediments for the past 3.3 Ma, we perform a least-squares linear regression between our new discrete $\%CaCO_3$ data (Figure 3C; n = 193), supplemented by the previously published $\%CaCO_3$ data (Figure 3B; n = 151 (Stein et al., 2009)), and 10 cm (5 point) running average of the L* data series (Figure 3D). The excellent linear correlation (r^2=+0.88, $p<0.001$; Figure 3D) between these two variables indicates that our orbital-resolution L*-based estimates of $\%CaCO_3$ are not strongly influenced by potential complicating factors (e.g. changing composition of the non-$CaCO_3$ fraction (Balsam et al., 1999)). This calibration is applicable to the task of generating a record of $\%CaCO_3$ for Site U1313 sediments of Pliocene through late Pleistocene age, but the

resultant %$CaCO_3$ record can only be used to estimate eolian dust fluxes prior to the late Pleistocene interval because of the error propagation associated with notable delivery of IRD during late Pleistocene ice-rafting events, most notably the extreme Heinrich events (see Section 3.3 (Stein et al., 2009; Naafs et al., 2013)). Fortunately, our focus is on the origin and temporal evolution of terrigenous MARs at our study site during the Pliocene where the linear fit is excellent and our new IRD record demonstrates that the terrigenous sediment component contains negligible (i.e. interglacial-like) ice-rafted sand-sized grains.

2.5. Radiogenic isotope data

The radiogenic isotope (Nd, Pb, Sr) composition of Atlantic Ocean sediment is well established as a tracer of both eolian sediment (e.g. Grousset et al., 1998; Abouchami and Zabel, 2003; Grousset and Biscaye, 2005) and ice rafted material (e.g. Revel et al., 1996; Grousset et al., 2001; Fagel et al., 2002; Fagel et al., 2004; Fagel and Matielli, 2011; Colville et al., 2011). These applications rely on regional differences in circum-North Atlantic Ocean geology as a function of age and tectonic (metamorphic) history.

To understand better the origin of the terrigenous component of Site U1313 Pliocene sediments, we have measured the Pb, Nd and Sr isotopic composition of carbonate-free bulk terrigenous samples selected from peak glacials and interglacials associated with the interval of iNHG (3.5–2.5 Ma; Mudelsee and Raymo (2005)). Sample processing closely followed Gutjahr et al. (2007). Approximately 0.5 g of crushed and homogenised bulk sediment was decarbonated using a Na acetate buffer, and absorbed metals were removed with a 1M $MgCl_2$ solution. Authigenic coatings were then removed using a 0.05 M hydroxylamine hydrochloride – 15 % acetic acid

– 0.03 M Na–EDTA solution buffered to pH 4 with analytical grade NaOH in two steps totalling 27 hours on a shaker table. Following removal of organic matter using hydrogen peroxide and aqua regia, samples were pressure-dissolved in a HF-HNO_3 mixture.

Pure samples of Pb, Nd and Sr were extracted using standard procedures. The Nd-isotope ($^{143}Nd/^{144}Nd$) and Pb-isotope ratios ($^{206}Pb/^{204}Pb$, $^{207}Pb/^{204}Pb$ and $^{208}Pb/^{204}Pb$) of our processed samples were measured at the University of Southampton using a multi-collector inductively coupled plasma mass spectrometer (MC-ICP-MS, Thermo Scientific Neptune). Neodymium isotopic compositions were obtained using the method of Vance and Thirlwall (2002) through adjustment to a $^{146}Nd/^{144}Nd$ value of 0.7219. Mass-bias corrected ratios were normalized to the given $^{143}Nd/^{144}Nd$ value (0.512115) of the standard JNdi-1 (Tanaka et al., 2000). Mass bias corrected Pb isotopic compositions were measured following a standard-sample bracketing approach normalizing Pb isotopic compositions of NBS981 to the values of Baker et al. (2004). The Strontium isotope composition ($^{87}Sr/^{86}Sr$) of these samples was also measured at the University of Southampton using a thermal ionisation mass spectrometer (ThermoFisher TRITON Plus). Total procedural blanks averaged 174pg, 106pg and 195pg for Nd, Sr and Pb, respectively. External precisions are calculated (at 2 standard deviations) as the reproducibility of the following standards: JNdi-1 (Nd), NBS 987 (Sr) and NBS 982 (Pb). Precision is 0.000007 (<0.15 εNd), 0.000015, 0.047, 0.022 and 0.062 for $^{143}Nd/^{144}Nd$, $^{87}Sr/^{86}Sr$, $^{206}Pb/^{204}Pb$, $^{207}Pb/^{204}Pb$ and $^{208}Pb/^{204}Pb$ respectively. For convenience Nd isotope ratios are reported in epsilon notation as:

$$\varepsilon_{Nd} = \left[\frac{^{143}Nd/^{144}Nd_{sample}}{^{143}Nd/^{144}Nd_{CHUR}} - 1 \right] \times 10^4$$

where $^{143}Nd/^{144}Nd_{CHUR}$ reflects the Chondrite Uniform Reservoir value of 0.512638 (Jacobsen and Wasserburg, 1980).

We assessed the provenance of terrigenous sediments deposited at Site U1313 by comparing their Pb, Sr and Nd isotopic compositions to equivalent radiogenic isotopic compositions of potential source regions, which are based on our compilation of discrete measurements made on circum-North Atlantic Ocean bedrock, terrestrial loess outcrop, atmospheric aerosols, and continental ice and dust source-proximal (core top and down-core) marine sediments and river samples (Figure 2a and 4 and Supplementary Information). Potential source areas for IRD deposited in the North Atlantic Ocean fall into three groups marked by a range of radiogenic isotope compositions (Figure 2a and 4 (c.f. Thierens et al., 2012)). The old, primarily Precambrian terranes of Greenland and North Eastern Canada (including the Labrador Sea, Hudson Strait and Baffin Bay) comprise the "Canadian Province" (Dawes et al., 2009). Paleocene to recent volcanic rocks found in Eastern Greenland, Iceland and the Faeroe Islands comprise the "Volcanic Province", local Azores volcanism may also contribute material of this composition. Together, areas with their corresponding compositions represent the high-latitude regions that constitute the most likely sites of early ice sheet growth (e.g. Winkler et al., 1999; DeConto et al., 2008). Lower-latitude ice rafting from Britain, Scandinavia or North America (the Appalachian terrane and Grenville Province in the region of the Gulf of Saint Lawrence) were important sources of ice-rafted material to the North Atlantic Ocean during the last glacial maximum (Watkins et al., 2007). Owing to their similarities in Pb and Nd-Sr isotope spaces, we group these three distinct geographic regions into a third province, intermediate in age to the two high-latitude provinces. Eolian material sourced from

277 the Sahara and North America has a similar geologic age and isotopic composition to
278 the Fenoscandinavian tectonic terranes and the Gulf of St Lawrence region of North
279 America, but is unequivocally distinct from high-latitude Volcanic Province material
280 and Precambrian and Proterozoic Canadian and Greenland terranes in Nd-Sr space.
281
282 **3. Results and Discussion**
283 *3.1. Stable isotope stratigraphy and sediment color*
284 The record of benthic $\delta^{13}C$ at Site U1313 shows only modest glacial-interglacial
285 variability with the exception of prominent excursions to low values during the large
286 benthic $\delta^{18}O$ glacials MIS 100, 98 and 96 (Figure 5). This result is consistent with the
287 record from predecessor Site 607 (Raymo et al., 1989), but the prominent
288 (inter)glacial $\delta^{13}C$ signal established in MIS 100 is more pronounced in our record.
289 Our record also resolves with higher fidelity earlier key glacials and illustrates, for
290 example, that MIS M2 (~3.3 Ma), the first prominent excursion in benthic $\delta^{18}O$ to
291 interrupt early Pliocene warmth, is not associated with a prominent benthic $\delta^{13}C$
292 excursion indicative of corrosive southern sourced waters.
293 Our L*-derived record of sediment $\%CaCO_3$ at Site U1313 is shown in
294 Figures 1A and 5 and reveals the expected North Atlantic pattern (lighter, $CaCO_3$-rich
295 sediments during interglacials and darker more terrigenous-rich intervals during
296 glacials), but the fidelity of the signal and its unambiguous correlation to our benthic
297 $\delta^{18}O$ series are remarkable back to 3.3 Ma (the base of our isotope record – Figure
298 5G). This relationship was postulated for Site U1313 based on shipboard correlation
299 of L* to the LR04 stack (Expedition 306 Scientists, 2006). Here we confirm, using
300 our co-registered signal ($\%CaCO_3$ and benthic $\delta^{18}O$ determined from the same
301 sediments) that variations in L* at Site U1313 track changes in benthic $\delta^{18}O$ at this

site across iNHG from 3.33 to 2.4 Ma. This result demonstrates that the onset of clear glacial-interglacial lithological cycles at this site took place at least 800 kyr earlier than the onset both of basin-wide ice rafting at MIS 100, 2.52 Ma, and of pronounced glacial-interglacial variability in benthic $\delta^{13}C$ at our study site (Figure 5B).

3.2. Abundance of the carbonate sedimentary component at Site U1313

Pliocene sediments at Site U1313 are characterized by small variations in color and $\%CaCO_3$ relative to the higher amplitude changes that characterize the late Pleistocene (Figure 1). High amplitude changes in Pleistocene $\%CaCO_3$ (and color) from the North Atlantic Ocean are often interpreted to reflect primarily changes in carbonate production and dilution by other sediment components (e.g. Lototskaya et al., 1998; Helmke and Bauch, 2001), while the lower amplitude $\%CaCO_3$ variations observed during the Pliocene at DSDP Sites 607 and 609 have been classically attributed to dissolution on glacial-interglacial timescales (Ruddiman et al., 1987). Our analysis, however, calls this classic interpretation into question. Calcareous microfossils are extremely well preserved in Pliocene sediments from Site U1313 with foraminifera fragment counts typically well within the zero ΔCO_3 range of Le and Shackleton (1992) (Figure 5A). The relationship between the fraction of $CaCO_3$ dissolved and that remaining is highly non-linear such that, when the $CaCO_3$ fraction is large, substantial $CaCO_3$ must be dissolved to achieve small percentage variations (Berger, 1971). For example, to generate a change in carbonate content of the order observed at Site U1313/607 between about 3.3 and 2.8 Ma (~95% to 85%, Figure 5G), about 60% of the initial $CaCO_3$ must be dissolved. Such substantial dissolution of $CaCO_3$ at Site U1313 is not consistent with the extremely well preserved calcareous microfossils observed in these sediments. Thus, in contrast to the classic

interpretation, $CaCO_3$ dissolution does not control carbonate content at Site U1313/607 prior to MIS 100 and cannot be used to assess changes in North Atlantic deep-water carbonate chemistry through time. Instead, the dominant controls must be calcite production and/or terrigenous dilution (Ruddiman and McIntyre, 1976; Ruddiman et al., 1987; Lototskaya et al., 1998; Helmke and Bauch, 2001).

A recently published record of alkenone accumulation from Site U1313 (Naafs et al., 2010) reveals the onset of high amplitude glacial-interglacial changes in alkenone accumulation, and therefore total export productivity (Bolton et al., 2010b; Bolton et al., 2011), from ~2.72 Ma (MIS G6). The orbital signal in the alkenone data, however, is of the wrong sign for carbonate productivity to control sediment color and $CaCO_3$ burial (alkenone accumulation peaks during glacials whereas $\%CaCO_3$ and color, L*, peak during interglacials; Figure 5C). Furthermore, our records demonstrate that terrigenous accumulation peaks during glacials throughout our study interval and not just from ~2.72 Ma onwards (Figure 5E). We conclude that the glacial-interglacial signal in Pliocene sediment color and $\%CaCO_3$ at Site U1313 is driven by addition of terrigenous material. Next we assess the potential mechanisms by which this terrigenous material might have been transported to our study site.

3.3. Radiogenic isotopes and sediment provenance

The Sr, Nd and Pb isotope composition of the bulk sediment terrigenous fraction deposited at Site U1313 during peak interglacial and glacial conditions during iNHG are shown in Figure 6. The Sr and Pb isotope composition of the samples analysed display a relatively small range of variability, with $^{87}Sr/^{86}Sr$ ranging from 0.71664 to 0.72561 and $^{206}Pb/^{204}Pb$ ranging from 18.20 to 18.97 (Fig 7A and C, respectively). Variation in εNd is more pronounced (ranging between -9.85 to -17.67), although

most values fall between -13.9 and -16 (Figure 7B). Two samples (corresponding to interglacials MIS G1 and 101) are indicative of volcanic material transported from East Greenland or Iceland, or from the Azores volcanic islands. Remarkably, aside from these two volcanically influenced exceptions, Nd, Sr and Pb isotope ratios show no systematic difference between samples selected from peak glacial and peak interglacial climate states (across a range in benthic $\delta^{18}O$ >1.5‰, Fig. 7D).

Based on the continuous presence of terrestrial leaf waxes in the Pliocene sediments at our study site (a tracer of eolian dust in marine sediments at Site U1313; Figure 5D), we know that at least some portion of the terrigenous fraction at Site U1313 is composed of eolian dust. This biomarker record exhibits fluxes akin to those observed for wind-blown leaf-waxes deposited in the Southern Ocean over the past ~4 Ma - where eolian dust is known to dominate the make-up of terrigenous sediments at ODP Site 1090 (Martínez-Garcia et al., 2011). Comparison of the Nd, Sr and Pb isotope composition of Site U1313 terrigenous sediments to those of potential source regions points to a definitive (non-volcanic) mid-latitude origin (Figures 6 and 7 and Supplementary Information). This observation is paleoclimatically powerful because it demonstrates that, prior to MIS G6 (>2.72 Ma), in a world characterized by only incipient high latitude NHG (e.g. Bintanja and van de Wal, 2008), eolian dust supply from the Sahara or North America is the only credible source capable of producing orbital-scale cyclical variations in terrigenous inputs to our study site. Our data are incompatible with a contribution from Greenland or Northern Canada, which are widely inferred to have been the nucleation points of the earliest northern hemisphere ice sheets (Winkler, 1999; Jansen et al., 2000; DeConto et al., 2008). In fact, where present, sand-sized IRD and volcanic grains occur in only trace numbers (typically 0 to <0.1 grains/g) in sediments older than MIS G4 at Site U1313, This finding,

together with the lack of a glacial-interglacial signal in our geochemical data, makes a high-latitude or even an improbable mid-latitude glacial origin for the bulk terrigenous fraction at Site U1313 untenable for sediments deposited prior to 2.7 Ma. These findings indicate that the bulk terrigenous sediment component deposited at Site U1313 between 3.3 Ma and 2.7 Ma is dominated by eolian dust.

We might expect a direct contribution from ice rafting to the terrigenous sediment component at Site U1313 during glacials between ~2.72 Ma and 2.4 Ma associated with the onset of significant NHG (Kleiven et al., 2002). As in the case of the older part of our record, however, our grain counts reveal, accumulation rates of sand-sized IRD in glacial sediments from MIS G4 onwards to be negligible (Figure 5). This result is in keeping with the location of Site U1313, situated far south (~41°N) of the late Pliocene IRD belt (centred on ~53°N; Bailey et al., 2013) and on only the southernmost fringe of the IRD belt even during the Last Glacial (Figure 1). This finding, together with, the consistent mid-latitude geochemical provenance indicated for terrigenous sediments deposited at Site U1313 leads us to conclude that, throughout our Pliocene record, the contribution made by IRD deposition shed from icebergs over site to the average radiogenic isotope composition of terrigenous sediments is insignificant in comparison to the major player, eolian dust. Similarly, despite evidence for abudant deposition of IRD in the higher latitude northeast North Atlantic Ocean sourced from high-latitude Archaean and Proterozoic-aged terranes during glacials since ~2.72 Ma (Bailey et al., 2013), the consistent mid-latitude geochemical provenance that we report here for the terrigenous fraction at Site U1313 makes it extremely unlikely that transport of fine-grained IRD beyond the contemporary iceberg front by ocean currents could be responsible for terrigenous deposition at our study site from MIS G6 onwards.

Similarities of the Nd and Sr isotopic composition of North American and Saharan eolian dust means that we must consider additional lines of evidence to pin down the source of the dust at Site U1313. Today, while most of the African-derived dust is driven westwards over the tropical North Atlantic by the Trade Winds, some dust is also transported northwards towards the North Atlantic, the Mediterranean and as far north as Northern Europe (Bergametti et al., 1989; Moulin et al., 1997; Kuss and Kremling, 1999; Kellog and Griffin, 2006). Three lines of evidence, however, support the notion that eolian dust deposition at our study site during iNHG is dominated by North American sources. First, spectral analysis of our record of terrigenous accumulation at Site U1313 reveals a dominant obliquity beat (with no strong precession signal) throughout our study interval that is in contrast to the pattern of variability in records of Saharan dust deposition (Fig. 8). Saharan dust deposition reveals the influence of obliquity from ~2.7 Ma, but precessional variability is important for at least the last 5 Ma (Tiedemann et al., 1994; DeMenocal, 2004)). Second, both modern wind trajectories (Figure 2B) and those modelled for both the last glacial maximum and Pliocene (Haywood et al., 2000; Hewitt et al., 2003; Pausata et al., 2011) indicate that Site U1313 is strongly influenced by intense westerly winds originating from the major present-day North American dust source region, the American Southwest (including all land between 125°W and 95°W and 25°N and 40°N) that incorporates the southwestern United States and parts of northern Mexico (Seager et al., 2007). Third, organic biomarker- and clay mineralogy-based provenance studies, respectively, independently link Plio-Pleistocene eolian derived terrestrial high plant waxes at Site U1313 (Naafs et al., 2012) and Holocene eolian-derived material across the central North Atlantic (Grousset and Chesselet, 1986) to North American sources.

427

428 *3.4. Records and mechanisms of North American eolian dust flux during Pliocene*
429 *iNHG*

430 Dust is both a signal and an agent of climate change (Martin et al., 1990; Kohfield and
431 Harrison, 2001; Mahowald et al., 2005; Winckler et al., 2008; Ganopolski et al., 2010;
432 Sun et al., 2010; McGee et al., 2010). To date, however, nearly all we know of the
433 history of eolian dust export from North America during Pliocene iNHG comes from
434 a single proxy biomarker record of terrestrial higher plant leaf wax (organic n-alkane)
435 deposition at Site U1313 (Naafs et al., 2012). That benchmark high-resolution record
436 shows that eolian-derived n-alkane and alkan-l-ols inputs to the North Atlantic Ocean
437 jumped to higher glacial values from ~2.7 Ma (MIS G6, Figure 5). Yet, these
438 biomarkers represent only a minor and often highly variable component of eolian dust
439 (Huang et al., 2000; Conte and Weber, 2003) so it is important to compare the proxy
440 biomarker record for dust deposition at Site U1313 with our record of variations in the
441 deposition of the terrigenous sediment component at this site.

442 Our record reveals that, while dust fluxes to our study site prior to the onset of
443 significant NHG at ~2.72 Ma are lower than those associated with Quaternary
444 glaciations, they are still high (up to 0.9 g/cm^2/ka) and unambiguously mimic global
445 climate (as recorded by benthic $\delta^{18}O$) back to at least 3.3 Ma (Figure 5E). The two
446 published biomarker records reveal that, from ~2.7 Ma onwards, glacial accumulation
447 of the organic fraction of North American dust increases significantly during glacials
448 at Site U1313 (Figure 5D). We are careful not to interpret our terrigenous record as a
449 pure signal of lithogenic dust deposition from this time because our records show
450 evidence for a contribution from ice rafting during glacials from MIS G4 onwards
451 (albeit extremely small, see Section 3.3). But our record of the bulk terrigenous flux

452 to Site U1313 places an upper limit on the potential magnitude of increase in eolian
453 dust flux to our study site that is possible during MIS G6 relative to background
454 interglacial values prior to this time: it can not be greater than a factor of about two
455 (Figure 5E). In fact, the peak fluxes that we record for the bulk terrigenous fraction
456 around 2.7 Ma (~2 g/cm^2/ka, Figure 5E) are similar to the lower end of the estimated
457 range of late Pleistocene glacial dust flux to the North Atlantic Ocean (2-5 g/cm^2/ka;
458 Maher and Denis, 2001).

459 The jumps in glacial accumulation in both the biomarker records and our
460 terrigenous record from MIS G6 (2.72 Ma) onwards (Figures 5D and 5E) strongly
461 suggest that the North American continent shifted abruptly into a distinctly more
462 Pleistocene-like cold stage regime (cold, arid, and windy) from MIS G6. One
463 potential mechanism for the sudden jump in dust inputs to our study site from 2.72
464 Ma is the development of large ice-sheets on North America from MIS G6 onwards as
465 inferred by Naafs et al. (2012). Large ice sheets advancing over regolith-rich Pliocene
466 terrains (Clark and Pollard, 1998) provide an attractive mechanism for delivering fine-
467 grained sediments to mid-latitude outwash plains for eolian entrainment (Ganopolski
468 et al., 2010), but three lines of evidence call this interpretation into question. (1)
469 Typically, the biomarker component of atmospheric dust becomes wind-entrained
470 through ablation from living vegetation assisted by sand blasting (eolian abrasion)
471 rather than by the deflation of soils and glacial outwash plains in dust source regions
472 (Huang et al., 2000; Conte and Weber, 2002; Schefuß et al., 2003). (2) Recent work
473 on the provenance of North Atlantic IRD (Bailey et al. 2013) and on Arctic climate
474 (Bringham-Grette, 2013) during iNHG indicates that major ice sheets (i.e. extending
475 into the mid latitudes) are unlikely to have been sustained in North America as early
476 as during MIS G6. In fact, our data show that dust inputs to Site U1313 were likely

substantial during cold stages well before MIS G6 with a particularly prominent peak in MIS M2 (Figure 5E), long before the existence of a large Laurentide ice sheet is tenable (De Schepper et al., 2013; Bringham-Grette et al., 2013). (3) Our radiogenic isotope data show a consistently mid-latitude provenance of the bulk terrigenous fraction at Site U1313 from 3.3 through 2.4 Ma regardless of glacial-interglacial state, thereby ruling out a significant high latitude contribution, even during MIS 100. These observations suggest that non-glaciogenic processes of Pliocene dust production, akin to those important during the last glacial maximum (e.g. increased wind intensity, enhanced aridity and reduced vegetation (Rea et al., 1994; Aleinikoff et. al., 1999; Mason 2001; Werner et al., 2002; Bettis et al., 2003; Winkler et al., 2002; Prospero et al., 2002; Bussaca et al., 2003 Mahowald et al., 2006; Aleinikoff et al., 2008; McGee et al., 2010)), are more important than suggested previously.

3.5. Non-linearity in the relation between biomarkers and terrigenous eolian dust deposition in the North Atlantic Ocean during Pliocene intensification of northern hemisphere glaciation.

In Figure 9 we present cross plots of our record of terrigenous mass accumulation at Site U1313 and the published biomarker records of Naafs et al. (2012) for our study interval (3.33-2.41 Ma). These cross plots reveal a close association between biomarker and terrigenous sediment accumulation at our study site but, in contrast to what is seen in other paleo-dust proxy records (Winckler et al., 2008) including other applications of the n-alkane technique (e.g. at South Atlantic Site 1090; Figure 9C; Martinez-Garcia et al., 2011), the relationships observed between the biomarkers and terrigenous fraction in Site U1313 are distinctly non-linear (e.g. Figure 9A vs. 9B). While stratigraphic comparison of these three records shows that they all display

jumps in glacial accumulation from MIS G6 (2.72 Ma) onwards (Section 3.4), the amplitude of this signal is about 3 to 8 times greater for biomarkers than for terrigenous inputs (Figure 10). The amplified jump in the biomarker records relative to the jump in the terrigenous record is particularly extreme during MIS 100 (2.52 Ma), especially in the record of n-alkan-1-ol accumulation (Figure 10). This observation underscores an important point: Non-linearity in the relation between the biomarkers and the lithogenic record cannot be explained by invoking the input of terrigenous material through additional mechanisms (ice rafting and volcanic inputs are the only other viable mechanisms at Site U1313) because additional terrigenous inputs would act to amplify our terrigenous record rather the biomarker record (ice rafting control on biomarker flux is not documented even during the extreme Heinrich events of the Late Pleistocene, Naafs et al. 2012). Furthermore, our records show that, where present (low values from MIS G4), IRD accumulation rates are always higher in glacials than in interglacials (sand-sized volcanic grains are extremely rare in Site U1313 sediments throughout our study interval; Figure 5). Thus, there is no way to explain amplification of the glacial jumps in the biomarker record (relative to the terrigenous fraction) by invoking decreases in IRD and/or volcanics inputs while a linear relation is maintained between biomarker and lithogenic dust. In other words, our records point to the unequivocal existence of some mechanism that acts to amplify the glacial jumps in the biomarker record relative to those in our terrigenous record.

Amplification of the glacial biomarker signal from MIS G6, and particularly during MIS 100 (Figure 10) points to increased efficiency of biomarker export/burial (especially in n-alkan-1-ols) and/or major shifts in vegetation biomes relative to preceding glacials. It seems an unlikely co-incidence that MIS 100 is the oldest glacial

for which there exists convincing evidence from diverse proxy records for the existence of a major Laurentide Ice Sheet (Bailey et al., 2010; 2013; Bringham-Grette et al., 2013) extending well into the mid-latitudes (39° north based on the terrestrial record of glacial tills; Balco and Rovey, 2010). We hypothesize that some combination of a southward shift of boreal and temperate forest biomes across North America, strengthening of wind-driven sand-blasting and perhaps precipitation-led increase in woody plant cover (woody thickening) in arid regions south of the Laurentide Ice Sheet front may be responsible for the amplified glacial jumps in the biomarker records, especially the extreme signal seen in MIS 100. Our hypothesis requires testing but is consistent with the interpreted response of the atmosphere and vegetation to ice sheet advance well into the mid-latitudes during the Last Glacial Maximum (LGM) (e.g., Clark & Pollard, 1998; Kutzbach et al., 1998; Clark et al., 1999; Thompson and Anderson 2000; Huang et al., 2001; Prentice et al., 2011; Bragg et al., 2013; Ullman et al., 2014).

3.6. Eolian dust deposition in the North Atlantic Ocean during the warm Pliocene.

We argue that the onset of clear glacial-interglacial cycles in sediment color is driven by changes in terrigenous dust accumulation at Site U1313 and that these cycles appear at least 800 kyr earlier than MIS 100 and well before significant iNHG commenced around 2.72 Ma. In Figure 11 we assess how far back into the Pliocene Epoch these signals extend by comparing sediment color reflectance and estimated lithogenic dust flux from Site U1313 to published climate records for the entire Plio-Pleistocene (to ~5.3 Ma, the base of LR04). The correspondence between sediment color at Site U1313 and global climate change registered by benthic $\delta^{18}O$ is remarkable. With the exception of one main interval of peak Pliocene warmth (4.3 to

552 ~4.0 Ma; Seki et al., 2012) when the sediment color reflectance record shows high
553 values with little orbital structure and a minor contribution from lithogenic dust can
554 be inferred, we observe the Pleistocene pattern (L* minima during glacials; maxima
555 during interglacials) at Site U1313 back to 5.3 Ma (the base of LR04, Fig. 11A).
556 In some respects, the signal of a minor lithogenic dust component during high
557 CO_2 warm Pliocene conditions is expected because climate model simulations (e.g.
558 Salzmann et al., 2008; 2013; Goldner et al., 2011) and paleo-data (e.g. Zarate and
559 Fasana, 1989; Thompson, 1991; Smith, 1994; Axelrod, 1997; Salzmann et al., 2008,
560 2009, 2013; Jimenez-Moreno et al., 2010) for the warm Pliocene, particularly for the
561 Mid-Piacenzian PRISM time-slab (Dowsett et al., 2012; Haywood et al., 2013),
562 indicate noticeably wetter than modern conditions in modern arid and semi-arid
563 regions, including the American Southwest. Yet in other respects our findings are
564 surprising because there is broad consensus among climate model predictions for the
565 future suggesting an increase in the expanse of arid to semi-arid mid-latitudes in a
566 warmer world, and that this transition should already be underway in North America
567 (e.g. Held and Soden, 2006; Seager et al., 2007; O'Gorman and Schneider, 2009).
568 Three main hypotheses have been suggested to explain the fundamental
569 discrepancy between climate model predictions for the next 50 to 100 years and the
570 model simulations of the warm Pliocene: (i) Differing boundary conditions, in
571 particular the effect on regional precipitation fields of a potentially markedly lower
572 elevation of the Pliocene Rocky Mountains (Wolf et al., 1997; Bonham et al., 2009)
573 prior to the mid Pliocene (Foster et al., 2010). (ii) Enhanced regional precipitation in
574 (southwest) North America relative to today in response to a warm eastern equatorial
575 Pacific (Fig. 11B) in an El Niño-prone world (Goldner et al., 2011). (iii) Fundamental
576 differences in the climate signal being modeled (equilibrium condition Pliocene

577 climates incorporate both short and long-term feedbacks associated with climate
578 sensitivity while predictions for the non-equilibrium condition 'climate transient' of
579 the coming 50 years necessarily incorporate only fast or Charney feedbacks
580 (Salzmann et al., 2009)).

581 Each of these hypotheses makes different predictions for the timing of the
582 onset of source aridification and dust generation spatially through Pliocene time,
583 thereby presenting a means to test their validity. For example, the disappearance of
584 summer wet flora in North American terrestrial records that span the Miocene-
585 Pliocene boundary on both sides of the Cascades and Sierra Nevada mountains
586 suggests that aridification of the American West through the Mio-Pliocene is unlikely
587 to be related to a rain shadow effect due to mountain uplift (Lyle et al., 2008).
588 Similarly, based on global terrestrial vegetation reconstructions, the picture of a
589 wetter-than present warm Pliocene appears to be too extensive (Salzmann et al., 2009;
590 2013) to support the suggested role of North American mountain orography. But
591 while terrestrial records of precipitation balance provide powerful insights into
592 Pliocene climate (Salzmann et al., 2013), they are, by their nature, discontinuous in
593 coverage and often suffer from age control limitations. Plio-Pleistocene data coverage
594 for mid-latitude North America, including for the core of the present-day arid
595 American Southwest, is extremely poor because of the lack of lacustrine deposits
596 generally and Pleistocene glacial erosion in the north (Salzmann et al., 2009; 2013).
597 The secular signal in the Site U1313 record is broadly consistent with the
598 hypothesized importance of warm sea surface temperatures in the Pliocene eastern
599 equatorial Pacific (Fig. 11). Yet, many differences between early Pliocene and
600 present-day climates of parts of Africa, Asia, and Australia do not resemble the
601 anomalies associated with canonical El Niño teleconnections (Cane and Molnar,

2007). Alongside model-based evaluation of the influence of fast versus slow feedbacks on precipitation balance and proxy reconstructions of the hydrological cycle, improved records of Pliocene dust deposition in well-dated marine sites recovered downwind from known Quaternary dust source regions will provide a valuable means to help understand the climatic response to sustained global warmth in the recent geological past.

4. Conclusions

We present Plio-Pleistocene records of sediment color, $\%CaCO_3$, foraminifer fragmentation, benthic $\delta^{13}C$, coarse lithic counts and the radiogenic isotope (Nd, Sr, Pb) composition of terrigenous sediment component from IODP Site U1313. We demonstrate that glacial-interglacial cycles in sediment color are unambiguously correlated to benthic $\delta^{18}O$ back to at least 3.3 Ma, and represent changes in sediment $\%CaCO_3$. Our new records of terrigenous and carbonate sediment accumulation rates, foraminifera fragmentation and benthic $\delta^{13}C$ show that these cycles are driven by enhanced glacial fluxes of terrigenous material and not glacial dissolution of carbonate material as previously interpreted.

On the basis of our radiogenic isotope data, we rule out a high-latitude origin for the terrigenous sediment component deposited at Site U1313 during our study interval and suggest that eolian dust sourced from mid latitude North America dominates clastic sediment deposition at this site during the Pliocene. This finding is consistent with previously published inferences on the provenance of an n-alkane biomarker proxy for dust inputs to our study site. Together with the biomarker records, our lithogenic data sets demonstrate that North America shifted abruptly to a distinctly more modern cold and arid glacial regime from MIS G6 with the

development of a Laurentide ice sheet extending well into the mid-latitudes by MIS 100. Yet the relation between the biomarker and lithogenic component of dust accumulation at Site U1313 is distinctly non-linear. Both records show a jump in glacial rates of accumulation from ~2.7 Ma onwards (during MIS G6) but the amplitude of this signal is about 3 to 8 times greater for biomarkers than for lithogenic dust and particularly extreme during MIS 100 (2.52 Ma).

The development of significant continental ice in the northern hemisphere during glacials from MIS G6 onwards undoubtedly had a profound impact on dust generation on North America. Our analysis, however, suggests that glacial grinding and transport of fine grained sediments to mid latitude outwash plains is not the fundamental mechanism controlling the magnitude of the flux of higher plant leaf waxes from North America to Site U1313 during iNHG. We hypothesize that some combination of latitudinal biome shift, strengthening of sand-blasting south of North American ice sheet front and perhaps precipitation-led woody thickening of arid regions in response to ice sheet advance towards the mid-latitudes may be responsible for the non-linearity observed. The secular pattern of change in the North Atlantic record indicates that there existed a minor lithogenic dust component at our study site during high-CO_2 peak Pliocene warm conditions (in contrast to climate model predictions for the future suggesting an increase in the expanse of arid to semi-arid zones in a warmer world). At least part of the discrepancy between climate model predictions for enhanced aridity of the mid latitudes over next 50 to 100 years and geologic observations for a warm wet Pliocene is likely attributable to fundamental differences in the climate signal being observed for the Pliocene versus that being modeled for future decades (equilibrium condition Pliocene climates versus transient non-equilibrium model predictions for the future). The form of secular change shown,

652 however, is broadly consistent with the hypothesized importance of warm sea surface
653 temperatures in the eastern equatorial Pacific during the Early Pliocene in bringing
654 about wetter-than-modern conditions in mid-latitude North America.
655
656 **5. Acknowledgements**
657 This research used samples provided by IODP, which was sponsored by the US
658 National Science Foundation and participating countries under management of Joint
659 Oceanographic Institutions, Inc. We thank the shipboard party of IODP Expedition
660 306. We also thank W. Hale and A. Wuelbers for help with sampling and D. Spanner,
661 M. Bolshaw and A. Michalik for laboratory assistance. We are grateful to the editor,
662 C. Hillaire-Marcel, two anonymous reviewers and Stijn de Schepper for detailed
663 constructive comments that helped to improve this manuscript. We thank Heiko
664 Pälike for his support and Ulrich Salzmann for discussions. I.B. is also grateful to UK
665 IODP for financial support for shipboard and post-cruise participation in IODP
666 Expedition 306. This study was supported by the Natural Environment Research
667 Council (NERC) in the form of a Ph.D studentship to D.C.L and a NERC UK IODP
668 grant NE/F00141X/1 to P.A.W and I.B. The data presented in this manuscript is
669 archived online at Pangaea (doi.pangaea.de/10.10.1594/PANGAEA.829428).
670
671 **6. References**
672 Abouchami, W., Zabel, M., 2003. Climate forcing of the Pb isotope record of
673 terrigenous input into the equatorial Atlantic. Earth Planet. Sci. Lett. 213, 221–
674 234.
675 Aleinikoff, J.N., Muhs, D.R., Sauer, R.R. & Fanning, C.M. 1999. Late Quaternary
676 loess in northeastern Colorado, II–Pb isotopic evidence for the variability of
677 loess sources. Geological Society of America Bulletin 111, 1876–1883.

678 Aleinikoff, J.N., Muhs, D.R., Bettis, E.A., Johnson, W.C., Fanning, C.M., Benton, R.,
679 2008. Isotopic evidence for the diversity of late Quaternary loess in Nebraska:
680 Glaciogenic and nonglaciogenic sources. Geological Society of America
681 Bulletin 120 (11–12), 1362–1377.
682 Andrews, J.T., 2000. Icebergs and iceberg rafted detritus (IRD) in the North Atlantic:
683 Facts and Implications. Oceanogr. 13, 100–108.
684 Asmerom, Y., Jacobsen, S.B., 1993. The Pb isotopic evolution of the Earth:
685 inferences from river water suspended loads. Earth and Planetary Science
686 Letters 115, 245–256.
687 Axelrod, D.I., 1997. Outline history of California vegetation, in: Terrestrial
688 Vegetation of California, edited by: Barbour, M. and Major, J., New York,
689 John Wiley and Sons, 139–193.
690 Bailey, I., Bolton, C.T., DeConto, R.M., Pollard, D., Schiebel, R., Wilson, P.A., 2010.
691 A low threshold for North Atlantic ice rafting from “low-slung slippery” late
692 Pliocene ice sheets, Paleoceanography 25, PA1212,
693 doi:10.1029/2009PA001736.
694 Bailey, I., Foster, G.L., Wilson, P.A., Jovane, L., Storey, C.D., Trueman, C.N., J.
695 Becker, J., 2012. Flux and provenance of ice-rafted debris in the earliest
696 Pleistocene sub-polar North Atlantic Ocean comparable to the last glacial
697 maximum, Earth and Planetary Science Letters 341–344, 222–233,
698 doi:10.1016/j.epsl.2012.05.034.
699 Bailey, I., Hole, G.M., Foster, G.L., Wilson, P.A., Storey, C.D., Trueman, C.N.,
700 Raymo, M.E., 2013. An alternative suggestion for the Pliocene onset of major
701 northern hemisphere glaciation based the geochemical provenance of North
702 Atlantic Ocean ice-rafted debris, Quaternary Science Reviews 75, 181–194,

703 doi:10.1016/j.quascirev.2013.06.004.
704 Baker, J., Peate, D., Waight, T., Meyzen, C., 2004. Pb isotopic analysis of standards
705 and samples using a 207Pb-204Pb double spike and thallium to correct for
706 mass bias with a double-focusing MC- ICP-MS. Chemical Geology 211, 275-
707 303, doi:10.1016/j.chemgeo.2004.06.030.
708 Balco G., Rovey C.W., II., 2010. Absolute chronology for major Pleistocene advances
709 of the Laurentide Ice Sheet. Geology 38, 795–798
710 Balsam, W.L., 1981. Late Quaternary sedimentation in the western North Atlantic:
711 Stratigraphy and paleoceanography. Palaeogeog. Palaeoclimatol. Palaeoecol.
712 35, 215–240.
713 Balsam, W.L., Deaton, B.C., Damuth, D.E., 1999. Evaluating optical lightness as a
714 proxy for carbonate in marine sediment cores. Mar. Geol. 161, 141–153.
715 Berger, W.H., 1971. Sedimentation of Planktonic Foraminifera. Mar. Geol. 11, 325-
716 358.
717 Bernstein, S., Kelemen, P.B., Tegner, C., Kurz, M.D., Blusztajn, J., Brooks, C.K.,
718 1998. Post-break up basaltic magmatism along the east Greenland tertiary
719 rifted margin. Earth and Planetary Science Letters 160, 845–862.
720 Biscaye, P.E., Grousset, F.E., Revel, M., Van der Gaast, S., Zielinski, G.A., Vaars, A.,
721 Kukla, G., 1997. Asian provenance of glacial dust (stage 2) in the Greenland
722 Ice Sheet Project 2 Ice Core. Summit, Greenland. Journal of Geophysical
723 Research 102, 26 76526 781.
724 Bergametti, G., Gomes, L., Coudegaussen, G., Rognon, P., Lecoustumer, M.N., 1989.
725 African Dust Observed over Canary Islands - Source-Regions Identification
726 and Transport Pattern for Some Summer Situations. J. Geophys. Res.-Atmos.
727 94**,** 14855–14864.

728 Bettis, E.A., Muhs, D.R., Roberts, H.M., Wintle, A.G., 2003. Last Glacial loess in the
729 conterminous USA. Quat. Sci. Revs. 22, 1907–1946.
730 Bintanja, R., van de Wal, R.S.W., 2008. North American ice-sheet dynamics and the
731 onset of 100,000-year glacial cycles. Nature 454, 869-872,
732 doi:1038/nature07158.
733 Bolton, C.T., Wilson, P.A., Bailey, I., Friedrich, O., Beer, C.J., Becker, J., Baranwal,
734 S., Schiebel, R., 2010a. Millennial-scale climate variability in the subpolar
735 North Atlantic Ocean during the late Pliocene. Paleoceanog. 25, PA4218,
736 doi:10.1029/2010PA001951.
737 Bolton, C.T., Lawrence, K.T., Gibbs, S.J., Wilson, P.A., Cleaveland, L.C., Herbert,
738 T.D., 2010b, Glacial–interglacial productivity changes recorded by alkenones
739 and microfossils inlate Pliocene eastern equatorial Pacific and Atlantic
740 upwelling zones. EPSL 295, 401–411.
741 Bolton, C.T., Lawrence, K.T., Gibbs, S.J., Wilson, P.A., Herbert, T.D., 2011. Biotic
742 and geochemical evidence for a global latitudinal shift in ocean
743 biogeochemistry and export productivity during the late Pliocene. EPSL 308,
744 (1–2), 200–210, http://dx.doi.org/10.1016/j.epsl.2011.05.046.
745 Bonham, S.G., Haywood, A.M., Lunt, D.J., Collins, M., Salzmann, U., 2009. El
746 Niño–Southern Oscillation, Pliocene climate and equifinality. Phil. Trans. R.
747 Soc. A (2009) 367, 127–156, doi:10.1098/rsta.2008.0212
748 Brigham-Grette, J. et al., 2013. Pliocene Warmth, Polar Amplification, and
749 Stepped Pleistocene Cooling Recorded in NE Arctic Russia. Science
750 340(6139), 1421-1427, doi:10.1126/science.1233137.
751 Bragg, F.J., Prentice, I.C., Harrison, S.P., Eglinton, G., Foster, P.N., Rommerskirchen,
752 F., Rullkötter, J., 2013. Stable isotope and modelling evidence for CO_2 as a

753 driver of glacial--interglacial vegetation shifts in southern Africa.
754 Biogeosciences 10(3), 2001–2010, www.biogeosciences.net/10/2001/2013/
755 doi:10.5194/bg-10-2001-2013.
756 Busacca, A.J., Beget, J.E., Markewich, H.W., Muhs, D.R., Lancaster, N., Sweeney,
757 M.R., 2004. Eolian sediments. In: Gillespie, A.R., Porter, S.C., Atwater, B.R.
758 (Eds.), The Quaternary Period in the United States. Elsevier, Amsterdam, The
759 Netherlands, pp. 275–310.
760 Busch, W.H., 1991. Analysis of wet-bulk density and sediment color cycles in
761 Pliocene-Pleistocene sediments of the Owen Ridge (Site 722) and Oman
762 Margin (Site 728). *In* Prell, W.L., Niitsuma, N., et al., Proc. ODP, Sci. Results,
763 117: College Station, TX (Ocean Drilling Program), 239–253.
764 Channell, J.E.T., Sato, T., Kanamatsu, T., Stein, R., Alvarez Zarikian C., 2010.
765 Expedition 303/306 synthesis: North Atlantic climate, Proceedings of the
766 Integrated Ocean Drilling Program 303/306,
767 doi:10.2204/iodp.proc.303306.214.
768 Chester, R. Elderfield, H., 1966. The infra-red determination of total carbonate in
769 marine carbonate sediments. Chem. Geol. 1, 277–290.
770 Clark, P.U., Pollard, D., 1998. Origin of the Middle Pleistocene Transition by ice
771 sheet erosion of regolith. Paleoceanography 13(1), 1–9,
772 doi:10.1029/97PA02660.
773 Clark, P. U., Alley, R.B., Pollard, D., 1999. Northern Hemisphere Ice-Sheet Influences
774 on Global Climate Change. Science 286, 1104–1111,
775 doi:10.1126/science.286.5442.1104
776 Cohen, R.S., O'Nions, R.K., 1982. The lead, neodymium and strontium isotopic
777 structure of ocean ridge basalts. Journal of Petrology 23, 299–324.

778 Cole, J.M., Goldstein, S.L., deMenocal, P.B., Hemming, S.R., Grousset, F.E., 2009.
779 Contrasting compositions of Saharan dust in the eastern Atlantic Ocean during
780 the last deglaciation and African Humid Period. Earth and Planetary Science
781 Letters 278, 257–266.
782 Colville, E.J., Carlson, A.E., Beard, B.L., Hatfield, R.G., Stoner, J.S., Reyes, A.V.,
783 Ullman, D.J., 2011. Sr-Nd-Pb isotope evidence for ice-sheet presence on
784 Southern Greenland during the last interglacial. Science 333, 620–623.
785 Conte, M.H., Weber, J.C., 2002. Long-range atmospheric transport of terrestrial
786 biomarkers to the western North Atlantic. Global Biogeochem. Cycles 16 (4),
787 1142, doi:10.1029/2002gb001922.
788 Conte, M.H., Weber, J.C., Carlson, P.J., Flanagan, LB., 2003. Molecular and carbon
789 isotopic composition of leaf wax in vegetation and aerosols in a northern
790 prairie ecosystem. Oecologia 135 (1), 67–77, doi:10.1007/s00442-002-1157-4.
791 Dawes, P.R. 2009. The bedrock geology under the Inland Ice: the next major
792 challenge for Greenland mapping Geol. Surv. Denmark Greenland Bull. 17,
793 57.
794 DeConto, R.M., Pollard, D., Wilson, P.A., Palike, H., Lear, C.H., Pagani, M., 2008.
795 Thresholds for Cenozoic bipolar glaciation. Nature 455, 652–656.
796 DeMenocal, P.B., 2004. African climate change and faunal evolution during the
797 Pliocene-Pleistocene. EPSL 220, 3–24.
798 De Schepper, S., Groeneveld, J., Naafs, B.D.A., Van Renterghem, C., Hennissen, J.,
799 Head, M.J., Louwye, S., Fabian, K., 2013. Northern Hemisphere Glaciation
800 during the Globally Warm Early Late Pliocene. PLoS ONE 8(12), e81508,
801 doi:10.1371/journal.pone.0081508
802 Dowsett, H.J. et al., 2012. Assessing confidence in Pliocene sea surface temperatures

803 to evaluate predictive models. Nature Clim. Change 2, 365–371, doi:
804 10.1038/NCLIMATE1455.
805 Ericson, D.B., Ewing, M., Wollin, G., Heezen, B.C., 1961. Atlantic deep-sea sediment
806 cores. Geol. Soc. Am. Bull. 72, 193–286.
807 Expedition 306 Scientists, 2006. Site 1313, in North Atlantic Climate, Proc. Integr.
808 Ocean Drill. Program, 303/306, doi:10.2204/iodp. proc.303306.112.2006.
809 Fagel, N., Innocent, C., Gariépy, C., Hillaire-Marcel., C., 2002. Sources of Labrador
810 Sea sediments since the Last Glacial Maximum inferred from Nd-Pb isotopes,
811 Geochim. Cosmochim. Acta 66, 2569–2581.
812 Fagel N., Hillaire-Marcel, C., Humblet, M., Brasseur, R., Weis, D., Stevenson, R.,
813 2004. Nd and Pb isotope signatures of the clay-size fraction of Labrador Sea
814 sediments during the Holocene: Implications for the inception of the modern
815 deep circulation pattern. Paleoceanography 19, PA3002, doi
816 10.1029/2003PA000993.
817 Fagel, N., Mattielli., N., 2011. Holocene evolution of deep circulation in the northern
818 North Atlantic traced by Sm, Nd and Pb isotopes and bulk sediment
819 mineralogy, Paleoceanography 26, PA4220, doi:10.1029/2011PA002168.
820 Farmer, G.L., Barber, D., Andrews, J., 2003. Provenance of late Quaternary ice-
821 proximal sediments in the North Atlantic: Nd, Sr and Pb isotopic evidence.
822 Earth and Planetary Science Letters 209, 227–243.
823 Ferretti, P., Crowhurst, S.J., Hall, M.A., Cacho, I., 2010. North Atlantic millennial-
824 scale climate variability 910 to 790 ka and the role of the equatorial insolation
825 forcing. Earth Planet. Sci. Lett. 293, 24–41. doi:10.1016/j.epsl.2010.02.016.
826 Ford, H.L., Ravelo, A.C., Hovan, S., 2012. A deep Eastern Equatorial Pacific
827 thermocline during the early Pliocene warm period, Earth and Planetary

828 Science Letters 355–356, 151–161,
829 http://dx.doi.org/10.1016/j.epsl.2012.08.027
830 Foster, G.L., Lunt, D.J., Parrish, R.R., 2010. Mountain uplift and the glaciation of
831 North America–a sensitivity study. Climate of the Past 6(5), 707-717.
832 Ganopolski, A., Calov, R., Claussen, M., 2010. Simulation of the last glacial cycle
833 with a coupled climate ice-sheet model of intermediate complexity. Clim. Past
834 6 (2), 229–244. doi:10.5194/cp-6-229-2010.
835 Gillette, D., 1999. A qualitative geophysical explanation for ‘‘hot spot’’ dust source
836 regions. Contrib. Atmos. Phys. 72, 67–77.
837 Goldner, A., Huber, M., Diffenbaugh, N., Caballero, R. 2011. Implications of the
838 permanent El Niño teleconnection “blueprint” for past global and North
839 American hydroclimatology. Clim. Past, 7, 723–743, 2011 www.clim-
840 past.net/7/723/2011/ doi:10.5194/cp-7-723-2011.
841 Goldstein, S.J., Jacobsen, S.B., 1988. Nd and Sr isotopic systematics of river water
842 suspended material: implications for crustal evolution. Earth and Planetary
843 Science Letters 87, 249–265, http://dx.doi.org/10.1016/0012-821X(88)90013-
844 1.
845 Grousset, F.E., Chesselet, R., 1986. The Holocene sedimentary regime in the northern
846 Mid-Atlantic Ridge region. Earth Planet. Sci. Lett. 78, 271–287.
847 Grousset, F.E., Parra, M., Bory, A., Martinez, P., Bertrand, P., Shimmield, G., Ellam,
848 R.M., 1998. Saharan wind regimes traced by the Sr–Nd isotopic composition
849 of subtropical Atlantic sediments: Last Glacial Maximum vs today. Quat. Sci.
850 Rev. 17, 395–409, http://dx.doi.org/10.1016/S0277-3791(97)00048-6.
851 Grousset, F.E., Cortijo, E., Huon, S., Hervé, L., Richter, T., Burdloff, D., Duprat, J.,
852 Weber, O., 2001. Zooming in on Heinrich layers. Paleoceanography 16, 240–

853 259, doi:10.1029/2000PA000559.
854 Grousset, F.E., Biscaye, P.E. 2005. Tracing dust sources and transport patterns using
855 Sr, Nd and Pb isotopes. Chem. Geol. 222, 149–167.
856 Gutjahr, M., Frank, M., Stirling, C.H., Klemm, V., van der Flierdt, T., Halliday., A.N.
857 2007. Reliable extraction of a deepwater trace metal isotope signal from Fe-
858 Mn oxyhydroxide coatings of marine sediments. Chem. Geol. 242, 351–370.
859 Hansen, H., Nielsen, T.F.D., 1999. Crustal contamination in Palaeogene east
860 Greenland flood basalts: plumbing system evolution during continental rifting.
861 Chemical Geology 157, 89–118, http://dx.doi.org/10.1016/S0009-
862 2541(98)00196-X.
863 Haywood, A.M., Sellwood, B.W., Valdes, P.J., 2000. Regional warming: Pliocene (3
864 Ma) paleoclimate of Europe and the Mediterranean. Geology 28, 10631066
865 Haywood, A.M., Dolan, A.M., Pickering, S.J., Dowsett, H.J., McClymont, E.L.,
866 Prescott, C.L., Salzmann, U., Daniel J. Hill, D.J., Stephen J. Hunter, S.J.,
867 Daniel J. Lunt, D.J., Pope, J.O., Valdes P.J., 2013. On the identification of a
868 Pliocene time slice for data–model comparison. Phil. Trans. R. Soc. A. 371,
869 20120515, doi:10.1098/rsta.2012.0515
870 Held, I.M., Soden, B.J., 2006. Robust responses of the hydrological cycle to global
871 warming. J. Climate 19, 5686–5699, doi:10.1175/JCLI3990.1.
872 Helmke, J., Bauch, H., 2001. Glacial-interglacial relationship between carbonate
873 components and sediment reflectance in the North Atlantic. Geo-Marine
874 Letters 21, 16–22, doi:10.1007/s003670100067.
875 Herbert, T.D., D'Hondt, S., 1990. Precessional climate cyclicity in Late Cretaceous–
876 early Tertiary marine sediments: a high resolution chronometer of Cretaceous–
877 Tertiary boundary events. EPSL 99, 263–275.

878 Hewitt, C.D., Stouffer, R.A., Broccoli, A.J., Mitchell, J.F.B, Valdes, P.J., 2003. The
879 effect of ocean dynamics in a coupled GCM simulation of the Last Glacial
880 Maximum. Clim. Dyn. 20 (2), 203–218.
881 Huang, Y.S., Dupont, L., Sarnthein, M., Hayes, J.M., Eglinton, G., 2000. Mapping of
882 C4 plant input from North West Africa into North East Atlantic sediments.
883 Geochimica et Cosmochimica Acta 64, 3505–3513.
884 Huang, Y.A., Street-Perrott, F.A., Metcalfe, S.E., Brenner, M., Moreland, M.,
885 Freeman, K.H., 2001. Climate change as the dominant control on glacial-
886 interglacial variations in C3 and C4 plant abundance. Science 293(5535),
887 1647–1651, doi:10.1126/science.1060143.
888 Ivanova, E., Schiebel, R., Singh, A.D., Schmiedl, G., Niebler, H.S, Hemleben, C.,
889 2003. Primary production in the Arabian Sea during the last 135000 years,
890 Palaeogeogr. Palaeoclimatol. Palaeoecol. 197, 61–82, doi:10.1016/S0031-
891 0182(03)00386-9.
892 Jacobsen, S.B., Wasserburg, G.J., 1980. Sm–Nd isotopic evolution of chondrites.
893 Earth and Planetary Science Letters 50 (1), 139–155.
894 Jansen, E., Sjoholm, J., 1991. Reconstruction of glaciation over the past 6 Myr from
895 ice-borne deposits in the Norwegian Sea. Nature 349, 600–603.
896 Jansen, E., Fronval, T., Rack, F., Channell, J.E.T., 2000. Pliocene-Pleistocene Ice
897 Rafting History and Cyclicity in the Nordic Seas During the Last 3.5 Myr.
898 Paleoceanog. 15, 709–721.
899 Jimenez-Moreno, G., Fauquette, S., and Suc, J. P., 2010. Miocene to Pliocene
900 vegetation reconstruction and climate estimates in the Iberian Peninsula from
901 pollen data. Review of Palaeobotany and Palynology 162, 403–415.
902 Juteau, M., Michard, A., Albarede, F., 1986. The Pb–Sr–Nd isotope geochemistry of

some recent circum-Mediterranean granites. Contributions to Mineralogy and Petrology 92, 331–340.

Kalnay, E., and Coauthors, 1996. The NCEP/NCAR 40-year Reanalysis Project. Bull. Amer. Meteor. Soc. 77, 437–472.

Kellogg, C.A., Griffin, D.W., 2006. Aerobiology and the global transport of desert dust. Trends in Ecology and Evolution 21(11), 638–644.

Kleiven–F, H., Jansen, E., Fronval, T., Smith, T.M., 2002. Intensification of Northern hemisphere glaciations in the circum Atlantic region (3.5-2.4 Ma) -ice-rafted detritus evidence. Palaeogeogr., Palaeoclimatol., Palaeoecol., 184, 213–223.

Kohfeld, K.E., Harrison, S.P., 2001. DIRTMAP: The geological record of dust. Earth Science Reviews 54: 81–114, http://dx.doi.org/10.1016/S0012-8252(01)00042-3.

Kokfelt T. F., Hoernle K. A. J., Hau□, F., Fiebig J., Werner R., Garbe-Schonberg D., 2006. Combined trace element and Pb–Nd–Sr–O isotope evidence for recycled oceanic crust (upper and lower) in the Iceland mantle plume. Journal of Petrology 47, 1705–1749.

Kuss, J., Kremling, K., 1999. Particulate trace element fluxes in the deep northeast Atlantic Ocean. Deep-Sea Research Part I-Oceanographic Research Papers 46**,** 149–169, http://dx.doi.org/10.1016/S0967-0637(98)00059-4.

Kutzbach, J.E., Gallimore, R., Harrison, S.P., Behling, P., Selin, R., Laarif, F., 1998. Climate and biome simulations for the past 21,000 years, Quaternary Science Reviews 17, 473–506, http://dx.doi.org/10.1016/S0277-3791(98)00009-2

Lawrence, K.T., Liu, Z.H., Herbert, T.D., 2006. Evolution of the eastern tropical Pacific through Plio-Pleistocene glaciation. Science 312, 79–83.

Lawrence, K.T., Herbert, T.D., Brown, C.M., Raymo, M.E., Haywood, A.M., 2009.

928 High-amplitude variations in North Atlantic sea surface temperature during the
929 early Pliocene warm period. Paleoceanog. 24. PA2218,
930 doi:10.1029/2008PA001669.
931 Lawrence, K.T., Sosdian, S., White, H.E., Rosenthal, Y., 2010. North Atlantic climate
932 evolution through the Plio-Pleistocene climate transitions. EPSL 300, 329-342.
933 Le, J., Shackleton, N.J., 1992. Carbonate dissolution fluctuations in the Western
934 Equatorial Pacific during the late Quaternary. Paleoceanog. 7**,** 21–42.
935 Lisiecki, L.E., Raymo, M.E., 2005, A Pliocene-Pleistocene stack of 57 globally
936 distributed benthic $\delta^{18}O$ records. Paleoceanog. 20, PA1003,
937 doi:10.1029/2004PA001071.
938 Lototskaya, A., Ziveri, P., Ganssen, G.M., van Hinte, J.E., 1998. Calcareous
939 nannofloral response to Termination II at 45°N, 25°W (northeast Atlantic).
940 Mar. Micropal. 34, 47–70.
941 Lunt, D.J, Foster, G.L., Haywood, A.M., Stone, E., 2008. Late Pliocene Greenland
942 glaciation controlled by a decline in atmospheric CO2 levels. Nature 454,
943 1102–1105.
944 Lyle, M., Barron, J., Bralower, T.J., Huber, M., Olivarez Lyle, A., Ravelo, A.C., Rea,
945 D.K., P.A. Wilson, P.A., 2008. Pacific Ocean and Cenozoic evolution of
946 climate. Rev. Geophys. 46, RG2002, doi:10.1029/2005RG000190.
947 Maher, B.A., Dennis, P.F., 2001. Evidence against dust mediated control of glacial-
948 interglacial changes in atmospheric CO_2. Nature 411, 176–180.
949 Mahowald, N.M., Baker, A.R., Bergametti, G., Brooks, N., Duce, R.A., Jickells, T.D.,
950 Kubilay, N., Prospero, J.M., Tegen, I., 2005. Atmospheric global dust cycle
951 and iron inputs to the ocean. Global Biogeochemical Cycles 19 (4), B4025,
952 doi:10.1029/2004GB002402.

953 Mahowald, N.M., Yoshioka, M., Collins, W. Conley, A., Fillmore, D., Coleman, D. ,
954 2006. Climate response and radiative forcing from mineral aerosols during the
955 glacial maximum, pre-industrial, current and doubled-carbon dioxide climates,
956 GRL 33, L20705, doi:10.1029/2006GL026126.
957 Martin, J.H., 1990. Glacial-interglacial CO2 change: The iron hypothesis,
958 Paleoceanog. 5(1), 1–13, doi:10.1029/PA005i001p00001.
959 Martínez-Garcia, A., Rosell-Melé, A., Jaccard, S.L., Geibert, W., Sigman, D.M., et al.,
960 2011. Southern Ocean dust–climate coupling over the past four million years.
961 Nature 476, 312–315, doi:10.1038/nature10310.
962 Maslin, M.A., Haug, G.H., Sarnthein, M., Tiedemann, R., Erlenkeuser, H., Stax, R.,
963 1995. Northwest Pacific Site 882: the initiation of Northern Hemisphere
964 glaciation. In: Rea, D.K., Basov, I.A., Scholl, D.W., Allan, J.F. (Eds.), Proc.
965 ODP, Sci. Res., 145, pp. 315–329.
966 Maslin, M.A., Li, X.S., Loutre, M.F., Berger, A., 1998. The contribution of orbital
967 forcing to the progressive intensification of Northern Hemisphere glaciation.
968 QSR 17, 411–426.
969 Mason, J.A., 2001. Transport direction of Peoria Loess in Nebraska and implications
970 for loess sources on the Central Great Plains. Quaternary Research 56, 79–86.
971 McGee, D., Broecker, W.S, Winckler, G., 2010. Gustiness: The driver of glacial
972 dustiness?, Quaternary Science Reviews 29 (17–18), 2340–2350,
973 doi:10.1016/j.quascirev.2010.06.009.
974 Millot, R., Allègre, C.J., Gaillardet, J., Roy, S., 2004. Lead isotopic systematics of
975 major river sediments: a new estimate of the Pb isotopic composition of the
976 Upper Continental Crust. Chemical Geology 203, 75–90.
977 Mix, A.C., Rugh, W., Pisias, N.G., Veirs, S., Leg 138 Shipboard Sedimentologists

(Hagelberg, T., Hovan, S., Kemp, A., Leinen, M., Levitan, M., Ravelo, C), and Leg 138 Scientific Party, 1992. Color reflectance spectroscopy: a tool for rapid characterization of deep-sea sediments. *In* Mayer, L., Pisias, N., Janecek, T, et al., Proc. ODP, Init. Repts., 138 (Pt. 1): College Station, TX (Ocean Drilling Program), 67–77.

Mix, A.C., Harris, S.E., Janecek, T.R., 1995. Estimating lithology from nonintrusive reflectance spectra: Leg 138. In: Pisias, N.G., Mayer, L.A., Janecek, T.R., Palmer-Julson, A., van Andel, T.H. (Eds.), Proc. of the Ocean Drill. Prog., Scientific Results, p. 138. 413–427.

Moulin, C., Lambert, C.E., Dulac, F., Dayan, U., 1997. Control of atmospheric export of dust from North Africa by the North Atlantic oscillation. Nature 387**,** 691–694.

Mudelsee, M., Raymo, M.E., 2005. Slow dynamics of the Northern Hemisphere glaciation. Paleoceanog. 20, PA4022, doi:10.1029/2005PA001153.

Naafs, B.D.A., Stein, R., Hefter, J., Khélifi, N., De Schepper, S., Haug G.H., 2010. Late Pliocene changes in the North Atlantic Current, Earth Planet. Sci. Lett. 298, 434–442, doi:10.1016/j.epsl.2010.08.023.

Naafs, B.D.A., Hefter, J., Acton, G., Haug, G.H., Martınez-Garcia, A., Pancost, R., Stein, R., 2012. Strengthening of North American dust sources during the late Pliocene (2.7 Ma). Earth Planet. Sci. Lett. 317, 8–19.

Ortiz, J.D., Mix, A., Harris, S., O'Connell, S., 1999. Diffuse spectral reflectance as a proxy for percent carbonate content in North Atlantic sediments. Paleoceanog. 14, 171–186.

O'Gorman, P., Schneider, T., 2009. Scaling of Precipitation Extremes over a Wide Range of Climates Simulated with an Idealized GCM. Climate 22, 5676–5685,

1003 doi:10.1175/2009JCLI2701.1.
1004 Pausata, F.S.R., Li, C., Wettstein, J.J., Kageyama, M., Nisancioglu, K.H., 2011. The
1005 key role of topography in altering North Atlantic atmospheric circulation
1006 during the last glacial period. Clim. Past 7 (4), 1089–1101. doi:10.5194/cp-7-
1007 1089–2011.
1008 Prospero, J.M., Ginoux, P., Torres, O., Nicholson, S., Gill, T., 2002. Environmental
1009 characterization of global sources of atmospheric soil dust identified with the
1010 Nimbus 7 Total Ozone Mapping Spectrometer (TOMS) absorbing aerosol
1011 product. Rev. Geophys. 40(1), 1002, doi:10.1029/2000RG000095.
1012 Prentice, I.C., Harrison, S.P., Bartlein, P.J., 2011. Global vegetation and terrestrial
1013 carbon cycle changes after the last ice age. New Phytologist 189, ISSN:0028-
1014 646X, 988–998.
1015 Raymo, M.E., Ruddiman, W.F., Backman, J., Clement, B.M., Martinson, D.G., 1989.
1016 Late Pliocene variation in Northern Hemisphere ice sheets and North Atlantic
1017 deep water circulation. Paleoceanog. 4, 413–446.
1018 Raymo, M.E., Hodell, D.A., Jansen, E., 1992. Response of deep ocean circulation to
1019 initiation of northern hemisphere glaciation (3-2 Ma). Paleoceanog. 7, 645–
1020 672.
1021 Rea, D.K., 1994. The paleoclimatic record provided by eolian deposition in the
1022 deepsea: the geologic history of wind. Reviews of Geophysics 32 (2), 159–
1023 195.
1024 Raymo, M.E., Oppo, D.W., Flower, B.P., Hodell, D.A., McManus, J., Venz, K.,
1025 Kleiven, K.F., McIntyre K., 2004. Stability of North Atlantic water masses in
1026 face of pronounced climate variability during the Pleistocene. Paleoceanog.
1027 19, PA2008, doi:10.1029/2003PA000921.

1028 Revel, M., Sinko, J.A., Grousset, F.E., Biscaye, P.E., 1996. Sr and Nd isotopes as
1029 tracers of North Atlantic lithic particles: paleoclimatic implications.
1030 Paleoceanography 11, 95–113.
1031 Ruddiman, W.F., Glover, L.K., 1972. Vertical Mixing of Ice-Rafted Volcanic Ash in
1032 North Atlantic Sediments. Geological Society of America Bulletin 83, 2817-
1033 2836.
1034 Ruddiman, W.F., McIntyre, A., 1976. "Northeast Atlantic Paleoclimatic Changes over
1035 the Past 600,000 Years. In *Investigation of Late Quaternary*
1036 *Paleoceanographaphy and Paleoclimatology* edited by R.M. Cline and J.D.
1037 Hays, Geol. Soc. of Am. Mem. 145, 111–146.
1038 Ruddiman, W.F., 1977. Late Quaternary Deposition of Ice-Rafted Sand in Subpolar
1039 North-Atlantic (Lat 40-Degrees to 65-Degrees-N). Geol. Soc. Am. Bull. 8,
1040 1813–1827.
1041 Ruddiman, W.F., McIntyre, A., Raymo, M.E., 1987. Paleoenvironmental results from
1042 North Atlantic Sites 607 and 609. Initial Reports DSDP 94, 855–878.
1043 Ruddiman, W.F., Raymo, M.E., 1988. Northern hemisphere climate regimes during
1044 the past 3 Ma: Possible tectonic connections, in *The Past Three Million Years:*
1045 *Evolution of Climatic Variability in the North Atlantic Region*, eds. N.J.
1046 Shackleton, R. G. West, and D. Q. Bowen, p. 1-20, Cambridge University P
1047 ress, England.
1048 Ruddiman, W.F., Raymo, M.E., Martinson, D.G., Clement, B.M., Backman, J., 1989.
1049 Pleistocene Evolution: Northern Hemisphere Ice Sheets and North Atlantic
1050 Ocean. Paleoceanog. 4, 353–412.
1051 Salzmann, U., Haywood, A., Lunt, D.J, Valdes, P., Hill, D.J., 2008. A new global
1052 biome reconstruction and data-model comparison for the Middle Pliocene.

1053 Global Ecology and Biogeography. 17(3). 432–447. ISSN 1466-822X.
1054 Salzmann, U. Haywood, A.M, Lunt., D.J. 2009. The past is a guide to the future?
1055 Comparing Middle Pliocene vegetation with predicted biome distributions for
1056 the twenty-first century. Phil. Trans. R. Soc. A 367, 189–204, doi:
1057 10.1098/rsta.2008.0200.
1058 Salzmann, U., Dolan, A.M., Haywood, A M., Chan W.-L., Hill, D.J., Abe-Ouchi, A.,
1059 Otto-Bliesner, B., Bragg, F., Chandler, M. A., Contoux, C., Dowsett, H.J., Jost,
1060 A., Kamae, Y., Lohmann, Lunt, D. J., Pickering, S.J., Pound M.J., Ramstein,
1061 G., Rosenbloom, N.A., Sohl, L., Stepanek, C., Ueda, H, Zhang, Z. (2013):
1062 Challenges in reconstructing terrestrial warming of the Pliocene revealed by
1063 data-model discord. Nature Climate Change.
1064 http://dx.doi.org/10.1038/nclimate2008.
1065 Seager, R., Ting, M., Held, I., Kushnir, Y., Lu, J., Vecchi, G., Huang, H.P., Harnik,
1066 N., Leetmaa, A., Lau, N.C., 2007. Model projections of an imminent transition
1067 to a more arid climate in southwestern North America. Science 316, 1181–
1068 1184, doi:10.1126/science.1139601.
1069 Seki, O., Foster, G.L., Schmidt, D.N., Mackensen, A., Kawamura, K., Pancost, R.D.,
1070 2010. Alkenone and boron-based Pliocene pCO2 records. Earth Planet. Sci.
1071 Lett. 292, 201–211, doi:10.1016/j.epsl.2010.01.037.
1072 Seki, O., Schmidt, D.N., Schouten, S., Hopmans, E.C., Sinninghe Damsté, J.S.,
1073 Pancost, R.D., 2012. Paleoceanographic changes in the Eastern Equatorial
1074 Pacific over the last 10 Myr. Paleoceanography 27, PA3224,
1075 doi:10.1029/2011PA002158.
1076 Schefuß, E., Ratmeyer, V., Stuut, J.B.W., Jansen, J.H.F., Sinninghe Damste , J.S.,
1077 2003. Carbon isotope analyses of n-Alkanes in dust from the lower

1078 atmosphere over the central eastern Atlantic. Geochimica et Cosmochimica
1079 Acta 67, 1757–1767.
1080 Shackleton, N.J., Backman, J., Zimmerman, H., Kent, D.V., Hall, M.A., Roberts,
1081 D.G., Schnitker, D., Baldauf, J.G., Desprairies, A., Homrighausen, R.,
1082 Huddlestun, P., Keene, J.B., Kaltenback, A.J., Krumsiek, K.A.O., Morton,
1083 A.C., Murray, J.W., Westbergsmith, J., 1984. Oxygen isotope calibration of the
1084 onset of ice-rafting and history of glaciation in the North-Atlantic region.
1085 Nature 307, 620–623.
1086 Smith, G.A., 1994. Climatic influences on continental deposition during late-stage
1087 filling of an extensional basin, southeastern Arizona. Geol. Soc. Am. Bull.
1088 106, 1212–1228, doi:10.1130/0016- 7606(1994)1061212:CIOCDD2.3.CO;2.
1089 Stein, R., Hefter, J., Grutzner, J., Voelker, A., Naafs, B.D.A., 2009. Variability of
1090 surface water characteristics and Heinrich-like events in the Pleistocene mid
1091 latitude North Atlantic Ocean: Biomarker and XRD records from IODP Site
1092 1313 (MIS 16-9). Paleoceanog. 24. PA2203, doi:10.1029/2008PA001639.
1093 Steph, S., Tiedemann, R., Groeneveld, J., Sturm, A., Nürnberg, D., 2006. Pliocene
1094 changes in tropical East Pacific Upper Ocean stratification: response to
1095 tropical gateways? Proc. Ocean Drilling Program Sci. Results 202, 1–51.
1096 Sun, Y., An, Z., Clemens, S.C., Bloemendal, J., Vandenberghe, J., 2010. Seven
1097 million years of wind and precipitation variability on the Chinese Loess
1098 Plateau. Earth and Planetary Science Letters 297(3), 525–535.
1099 Tanaka, T., Togashi, S., Kamioka, H., Amakawa, H., Kagami, H., Hamamoto, T.,
1100 Yuhara, M., Orihashi, Y., Yoneda, S., Shimizu, H., Kunimaru, T., Takahashi,
1101 K., Yanagi, T., Nakano, T., Fujimaki, H., Shinjo, R., Asahara, Y., Tanimizu,
1102 M., Dragusanu, C., 2000. JNdi-1: a neodymium isotopic reference in

consistency with LaJolla neodymium. Chemical Geology 168 (3–4), 279–281, http://dx.doi.org/10.1016/j.chemgeo.2007.03.021.

Taylor, S.R., McLennan, S.M., McCulloch, M.T., 1983. Geochemistry of loess, continental crustal composition and crustal model ages. Geochimica et Cosmochimica Acta 47, 1897–1905.

Thierens, M., Pirlet, H., Colin, C., Latruwe, K., Vanhaecke, F., Lee, J.R., Stuut, J.-B., Titschack, J., Huvenne, V.A.I., Dorschel, B., Wheeler, A.J., Henriet, J.-P., 2012. Ice-rafting from the British-Irish ice sheet since the earliest Pleistocene (2.6 million years ago): implications for long-term mid-latitudinal ice-sheet growth in the North Atlantic region. Quaternary Science Reviews 44, 229–230, doi:10.1016/j.quascirev.2010.12.020.

Thompson, R.S., 1991. Pliocene environments and climates in the western U.S. Quat. Sci. Rev. 10, 115–132.

Thompson, R.S., Anderson, K.H., 2000. Biomes of western North America at 18,000, 6000 and 0 ^{14}C yr PB reconstructed from pollen and packrat midden data. J. Biogeogr. 27, 555–584.

Tiedemann, R. Sarnthein, M., Stein, R., 1989. Climatic changes in the western Sahara: Aeolo-marine sediment record of the last 8 million years (Sites 657-661). ODP, Sci. Results, 108: College Station, TX (Ocean Drilling Program), 241–277.

Tiedemann, R. Sarnthein, M., Shackleton, N.J., 1994. Astronomic timescale for the Pliocene Atlantic δ18O and dust flux records of Ocean Drilling Program Site 659, Paleoceanog. 9, 619–638.

Torrence, C., Compo., G.P., 1998. A practical guide to wavelet analysis, Bull. Am. Meteorol. Soc. 79, 61–78.

1128 Ullman, D.J., LeGrande, A.N., Carlson, A.E., Anslow, F.S., Licciardi, J.M., 2014.
1129 Assessing the impact of Laurentide Ice Sheet topography on glacial climate.
1130 Clim. Past 10, 487–507, doi:10.5194/cp-10-487-2014.
1131 Vance, D., Thirlwall, M., 2002. An assessment of mass discrimination in MC-ICPMS
1132 using Nd isotopes. Chemical Geology 185 (3–4), 227–240,
1133 http://dx.doi.org/10.1016/S0009-2541(01)00402-8.
1134 Washington, R., Todd, M., Middleton, N.J., Goudie, A.S., 2003. Dust- storm
1135 source areas determined by the total ozone monitoring spectrometer and
1136 surface observations. Ann. Assoc. Am. Geogr. 93(2), 297–313.
1137 Watkins, S.J., Maher, B.A., Bigg, G.R., 2007. Ocean circulation at the Last
1138 Glacial Maximum: A combined modeling and magnetic proxy-based study.
1139 Paleoceanography 22, PA2204, doi:10.1029/2006PA001281.
1140 Werner, M., Tegen, I., Harrison, S.P., Kohfeld, K.E., Prentice, I.C., Balkanski, Y.,
1141 Rodhe, H., Roelandt, C., 2002. Seasonal and interannual variability of the
1142 mineral dust cycle under present and glacial climate conditions. Journal of
1143 Geophysical Research 107 (D24). doi:10.1029/2002JD002365
1144 Winkler, A., 1999. The climate history of the high northern latitudes since the middle
1145 Miocene: Indications from sedimentological and clay mineralogical analyses
1146 (ODP leg 151, central Fram strait), Reports on Polar Research, Alfred Wegener
1147 Institute for Polar and Marine Research, Bremerhaven, Germany, 344, 117 pp.
1148 Winkler, A., Wolf-Welling, T., Stattegger, K., & Thiede, J., 2002. Clay mineral
1149 sedimentation in high northern latitude deep-sea basins since the Middle
1150 Miocene (ODP Leg 151, NAAG). International Journal of Earth Sciences
1151 91(1), 133–148.
1152 Winckler, G., Anderson, R.F., Fleisher, M.Q., McGee, D. Mahowald, N., 2008.

Covariant glacial-interglacial dust fluxes in the Equatorial Pacific and Antarctica. Science 320, 93–96, doi: 10.1126/science.1150595.

Wolfe J.A., Schorn H.E., Forest C.E., Molnar P., 1997. Paleobotanical evidence for high altitudes in Nevada during the Miocene, Science 276, 1672–1675, doi:10.1126/science.276.5319.1672.

Zarate, M.A., Fasano, J.L., 1989. The Plio–Pleistocene record of the central eastern Pampas, Buenos Aires province, Argentina: the Chapadmalal case study. Palaeogeogr., Palaeoclimatol., Palaeoecol. 72, 27–52. doi:10.1016/0031-0182(89)90130-2.

Figure captions

Figure 1. Lithostratigraphic cycles in North Atlantic deep-sea sediments of Plio-Pleistocene age in multiple drill sites as revealed by published physical property records. Sites arranged (from top to bottom) in order of increasing water depth. Note the existence of clear rhythmic cycles significantly earlier than MIS 100, the inferred glacial for the onset of basin-wide ice rafting. The data presented in the bottom panel **(A)** were originally compiled by Ruddiman et al. (1987, their Figure 3), although we substitute their record from DSDP Site 607 with our higher resolution proxy record from IODP Site U1313 (See Section 2.4 for methods). Those authors concluded that %$CaCO_3$ variability at pelagic DSDP Sites 607 (U1313) and 609, but not at the shallower DSDP Site 552, prior to Gauss/Matuyama boundary time was attributable to sea floor $CaCO_3$ dissolution, a consequence of the influence of corrosive poorly ventilated glacial intermediate waters in the North Atlantic. Top panel **(B)** shows data generated from additional shallow sites drilled after the Ruddiman et al., (1987) study (pelagic Site 982 (Shipboard Scientific Party, 1996), drift Site 980/981 (Ortiz et al.,

1999)). Note that the timing of the initiation of marked lithological cycles in the North Atlantic drill sites is not a simple function of water depth suggesting that $CaCO_3$ dissolution is not the principle origin of these cycles (see text). The horizontal black/white bars in each panel denote paleomagnetic (sub)chronozone boundaries (Cande and Kent, 1995): B = Brunhes, M = Matuyama, G = Gauss, K = Keana, Ma = Mammoth and Gil = Gilbert.

Figure 2. North Atlantic region showing location of IODP Site U1313 relative to other drill sites referred to in the text **(A)** and mean April to September (the 'dust season'; Prospero et al., 2002) surface wind vectors (**B**; image source http://www.esrl.noaa.gov/psd/ (Kalnay et al., 1996)). Also shown in (A) is the last glacial maximum IRD-belt (stippled area) of Ruddiman (1977), relevant principal surface-ocean current systems (adapted from Kleiven et al., 2002) and average radiogenic isotope composition of potential source regions of terrigenous sediments deposited at Site U1313 (based on data shown in Figure 4).

Figure 3. Relationship between IODP Site U1313 sediment color (L*) and calcium carbonate (%$CaCO_3$) content. Global benthic oxygen isotope stack for the Plio-Pleistocene, the LR04 (Lisiecki and Raymo, 2005) and published benthic oxygen isotope data for IODP Site U1313 **(A)**; discrete %$CaCO_3$ measurements for late Pleistocene (**B**, black circles, Stein et al., (2009), n = 151) and late Pliocene and earliest Pleistocene (**C**, red circles, this study, n = 193) and our high resolution estimate of sediment %$CaCO_3$ (against meters composite depth, mcd) based on least squares linear regression of L* (5-point, 10 cm, moving average) onto discrete %$CaCO_3$ measurements **(D)**. Data corresponding to North Atlantic Hudson Strait Heinrich-like events (vertical grey bars in B labelled HE), for which the relationship

between L* and %$CaCO_3$ breaks down, are excluded from our least square regression. We identified Heinrich Layers at Site U1313 following Stein et al. (2009), based on their high (>500 cps) x-ray diffraction-derived dolomite concentrations. The horizontal black/white bars in each panel denote paleomagnetic (sub)chronozone boundaries (Cande and Kent, 1995): B = Brunhes, M = Matuyama, G = Gauss, K = Keana, Ma = Mammoth, Gil = Gilbert, C = Cochiti, N = Nunivak and S = Sidufjall. Depth range of chronozone boundaries shown in (B) and (C) based on shipboard measurements (Expedition 306 Scientists, 2006).

Figure 4. Characterisation of likely sources of terrigenous sediment to Site U1313 in Nd-Sr **(A)** and Pb-Pb **(B & C)** spaces. These fields are based on modern bedrock, loess, river sediment and aerosol data, and modern to LGM ice sheet/dust source proximal sediment core data. Potential sources constitute high-latitude material from Greenland and Northern Canada (the Canadian Province, Blue), volcanic material from Eastern Greenland and Iceland (Red, together with the Canadian Province this represents the most likely source of ice rafted material), mid-latitude material from Europe and the Gulf of St. Lawrence (purple) that is unlikely to be a significant source of ice-rafted material prior to significant northern hemisphere glaciation and potential aeolian sources from North America and the Sahara (green and yellow bubbles, respectively). Fields based on data from (also see Supplementary Information, Figures S1–S5): Abouchami and Zabel. (2003), Aleinkoff et al. (1999), Aleinkoff et al. (2008), Asmerom and Jakobsen (1993), Bernstein et al., (1998), Biscaye et al. (1997), Cohen and O'Nions (1982), Cole et al. (2009), Farmer et al. (2003), Goldstein and Jacobsen (1988), Grousset et al. (1988), Grousset et al. (2001), Hansen and Nielsen (1999), Juteau et al. (1986), Kokfelt et al. (1983), Kokfelt et al.

(2006), Millot et al. (2004), Revel et al. (1996).

Figure 5. Paleoceanographic records from IODP Site U1313 for the late Pliocene and earliest Pleistocene: **(A)** Foraminifera fragments as a percentage of total foraminifera plus fragments observed in the >150μm fraction (Ivanova et al., 2003). Overall, the carbonate material from this site is exceptionally well preserved. Modest increases in fragmentation are observed, however, during glacial periods from ca. 2.52 Ma onwards, demonstrating that more corrosive conditions existed at this site during glacials MIS 100, 98 and 96. For reference, we have included a line that approximates $\Delta(CO_3^{2-}) = 0$ in terms of percentage fragmentation based on Le and Shackleton (1992); **(B)** Benthic foraminiferal $\delta^{13}C$, measured on *Cibicidoides wuellerstorfi* (this study); **(C)** Alkenone mass accumulation rates, a productivity proxy (Naafs et al., 2010); **(D)** Mass accumulation rates, MAR, of n-alkanes and C26-alkan-1-ol, aeolian derived biomarkers (Naafs et al., 2012); **(E)** Calculated MAR of terrigenous material (this study); **(F)** Concentration of ice rafted coarse lithics (Ice rafted detritus, IRD, >150 μm, excluding volcanics, which are only ever present in trace numbers). Transparent grey box shows the range of peak glacial values estimated for high-latitude North Atlantic Ocean DSDP Site 611 between MIS G6-100 (~2.72-2.5 Ma; Bailey et al., 2013). Overall, coarse lithic content of iNHG sediments at Site U1313 is extremely low (<50 grains g^{-1}) and prior to MIS 100 never higher than 5 grains g^{-1} (contrast with extremely high concentrations of 1500-5000 g^{-1} at Site 611); **(G)** Benthic $\delta^{18}O$ (Bolton et al., 2010) and L* derived $\%CaCO_3$ (this study), a remarkable correlation is seen. All data plotted on age model of Bolton et al. (2010). All MAR data shown estimated (as MAR = component abundance x linear sedimentation rate x dry bulk density) using sedimentation rates based on the age model of Bolton et al.

(2010) and dry-bulk densities from shipboard determined GRAPE wet-bulk density data following the approach of Maslin et al. (1995). MARs shown in (C) and (D) recalculated on this basis using published datasets, but do not differ appreciably from original fluxes reported by Naafs et al. (2012). The horizontal black/white bars at the base of the figure denote paleomagnetic chronozone boundaries (Cande and Kent, 1995): M = Matuyama, G = Gauss, K = Keana and Ma = Mammoth.

Figure 6. Pb **(A & B)** and Nd-Sr **(C)** isotope composition of Plio-Pleistocene IODP Site U1313 bulk terrigenous sediments and range of radiogenic isotope values for potential terrigenous sources (as compiled in this study, see supplementary information, Figures S1–S5). Data from interglacial (triangles) and glacial (circles) samples are highlighted. Data uncertainty (at 2σ) is plotted, but usually smaller than symbols shown.

Figure 7. Time series of the radiogenic isotope composition of bulk terrigenous sediments deposited at IODP Site U1313: $^{87}Sr/^{86}Sr$ **(A)** εNd **(B)**, $^{206}Pb/^{204}Pb$ **(C)**. Benthic $\delta^{18}O$ stratigraphy for Site U1313 (Bolton et al., 2010) shown for reference. Grey dashed lines highlight relationship between data in (A-C) and glacial and interglacial marine isotope stages shown in **(D)**. Data uncertainty (at 2σ) in A-C is smaller than symbols used. The radiogenic isotope composition of source regions shown on right hand side of figure (median – black line, 66th percentile – box, 95th percentile – "whisker", outlying data-points marked as small crosses) are determined from data shown in Figure 4. Horizontal green lines denote the median of North American loess measurements, concluded to be the dominant source of Site U1313 terrigenous sediments (see main text). For comparison, Nd and Sr isotope

1279 measurements from last glacial maximum ice rafting events at nearby drill cores
1280 (Sites SU90-08 and SU90-09 (Revel et al., 1996; Grousset et al., 2001)) are shown in
1281 (A) and (B). These data reveal extensive variability during the last glacial cycle (from
1282 -5.8 to -40.9 εNd, 0.72904 to 0.71662 $^{87}Sr/^{86}Sr$) and demonstrate that the radiogenic
1283 isotope systems studied are sensitive to large ice rafted debris inputs when present. Ice
1284 rafted debris is first observed at Site U1313 during MIS G6 (labelled in D). The
1285 horizontal black/white bars at the base of the figure denote paleomagnetic chronozone
1286 boundaries (Cande and Kent, 1995): M = Matuyama, G = Gauss, K = Keana and Ma
1287 = Mammoth.
1288
1289 **Figure 8.** Wavelet analysis of North Atlantic ODP Site 659 terrigenous accumulation
1290 rate **(A)** (Tiedemann et al., 1994), and Site U1313 terrigenous accumulation rate **(B)**
1291 and benthic oxygen isotopes (Bolton et al., 2010) **(C)**. Wavelet spectra estimated
1292 following (Torrence and Compo, 1998). Solid black lines in each panel enclose
1293 regions of >95% confidence, based on a red-noise model (Torrence and Compo,
1294 1998). Within light shaded areas of panel B and C confident interpretation cannot be
1295 drawn due to edge effects (Torrence and Compo, 1998). These effects are not visible
1296 in (A) because we show only a central portion of a 5.3 Ma record analysed.
1297 Horiztonal dashed grey lines on each panel labeled with 19, 23, 41 and 100 pick out
1298 dominant periodicities of orbtial cycles. The dominant 20 ka, precessional cyclicity
1299 seen in Saharan dust inputs to Site 659 is not found in the mass accumulation rate of
1300 terrigenous sediment at Site U1313. The age model used for Site 659 is based on that
1301 published in Tiedemann et al. (1994). Re-analysis of the Site 659 terrigenous
1302 accumulation rate record following retuning of its benthic $\delta^{18}O$ stratigraphy to the
1303 LR04 stack (Lisiecki and Raymo, 2005) does not remove the strong 20 ka

precessional cyclicity shown in panel A (see Supplementary Information).

Figure 9. Cross plots of late Pliocene and earliest Pleistocene (3.33–2.41 Ma) IODP Site U1313 paleoceanographic and paleoclimate proxies: **(A)** Non-linear relationship between accumulation rates of terrigenous sediment (this study, interpreted as dominantly eolian dust) and dust-derived organic biomarkers (Naafs et al., 2012); **(B)** Non-linear relationship between global climate as recorded by benthic oxygen isotopes at Site U1313 (Bolton et al., 2010) and dust-derived organic biomarkers (Naafs et al., 2012); **(C)** Linear relationship between inferred eolian dust accumulation rates and dust-derived biomarker accumulation rates at Southern Ocean ODP Site 1090 (42°54.8′S, 8°54.0′E (Martinez-Garcia et al., 2011)). **(D)** Linear relationship between Site U1313 benthic oxygen isotopes (Bolton et al., 2010) and accumulation rates of terrigenous sediment (interpreted here as dominantly eolian dust). Note, we only plot data older than 2.41 Ma for Site U1313 when we can be confident that the bulk terrigenous sediment component at this site is dominated by eolian dust. Site 1090 data represent the last 4 Ma of aeolian dust deposition at this site. Biomarker accumulation rates used in this figure come from those plotted in Figure 4. Cross-plots in (A), (B) and (D) generated following linear interpolation of the terrigenous mass accumulation rate record to match the relatively lower resolution of the biomarker and benthic $\delta^{18}O$ data.

Figure 10. Time series of the ratio of accumulation rates of C26-alkan-1-ol and n-Alkane (Naafs et al., 2012) to terrigenous sediments at Site U1313. Both ratio time series are normalized to the average ratio observed for the Piacenzian PRISM time-slab (defined as 3.025-3.264 Ma). Biomarker accumulation rates used are the same as

1329 those shown in Figure 5. Our higher-resolution record of terrigenous sediment
1330 accumulation rate is linearly interpolated to match the resolution of the biomarker
1331 records. The Site U1313 oxygen isotope stratigraphy (Bolton et al., 2010) is shown
1332 for reference, with key glacial marine isotope stages (M2, G6 and 100) labelled. Note,
1333 during glacial periods biomarker accumulation rates are enhanced relative to
1334 accumulation rates of bulk terrigenous material. The horizontal black/white bars at the
1335 base of the figure denote paleomagnetic chronozone boundaries (Cande and Kent,
1336 1995): M = Matuyama, G = Gauss, K = Keana and Ma = Mammoth.
1337
1338 **Figure 11.** The relationship between Site U1313 sediment lightness (L*) and globally
1339 representative benthic $\delta^{18}O$, the LR04 (Lisiecki and Raymo, 2005) **(A)** and proxy
1340 indicators of the evolution of eastern equatorial Pacific (EEP) sea-surface temperature
1341 (**B**, based on alkenones from ODP Site 846 (Lawrence et al., 2006)) and sub-surface
1342 temperature (**C**, based on Mg/Ca ratios in foraminifer from ODP Sites 848, 849 and
1343 853 (Ford et al., 2012); ODP Site 1241 (Steph et al., 2006)). Horizontal dashed blue
1344 line in (B) corresponds to Holocene sea-surface temperature average for ODP Site
1345 846 (Lawrence et al., 2006). During the early Pliocene the mid latitudes of North
1346 America were wetter and warmer than present (Goldner et al, 2011). Note the warm
1347 temperatures of the EEP Ocean (associated with small zonal equatorial SST gradients
1348 (Ford et al., 2012), a state referred to as permanent El Niño-like (implies nothing
1349 about interannual variability). It is hypothesised that the development of the EEP cold
1350 tongue at this time and a subsequent poleward shift in the Pacific jet stream led to the
1351 aridification of North America (Goldner et al., 2011). Note that L* at Site U1313, a
1352 proxy for sediment eolian content is unambiguously correlated to global climate
1353 (LR04) back to 3.3 Ma and intermittantly so probably back to 5.3 Ma (base of LR04),

the notable exception being ~4.3 to 4 Ma (see main text). For sediments older than 3.3 Ma, our manual graphical correlation of Site U1313 and LR04 is based on tuning between constraints provided by shipboard determination of depths to paleomagnetochronozone boundaries (Expedition 306 Scientists, 2006). Age model control for ~2.4-3.3 Ma and <2.4 Ma, respectively, come from Bolton et al. (2010) and Naafs et al. (2012) and Expedition 306 Scientists (2006). The horizontal black/white bars at the top and base of the figure denote paleomagnetic chronozone boundaries (Cande and Kent, 1995): B = Brunhes, M = Matuyama, G = Gauss, K = Keana, Ma = Mammoth, Gil = Gilbert, C = Cochiti, N = Nunivak, S = Sidufjall and T = Thvera.

Figure 1

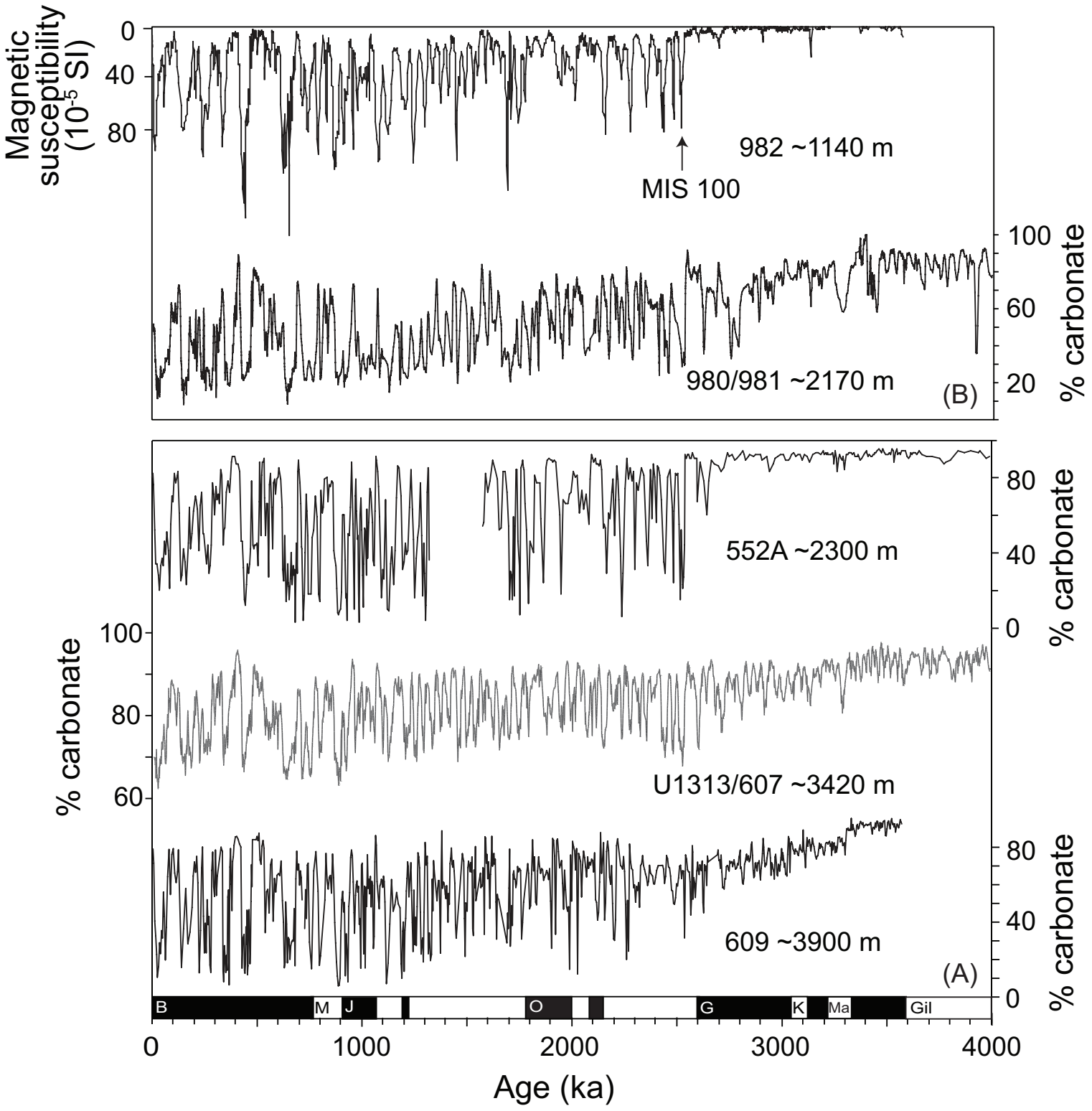
Magnetic susceptibility (10^{-5} SI)
0
40
80
982 ~1140 m
MIS 100
980/981 ~2170 m
(B)
100
60
20
% carbonate
552A ~2300 m
U1313/607 ~3420 m
609 ~3900 m
(A)
80
40
0
100
80
60
% carbonate
B
M
J
O
G
K
Ma
Gil
0
1000
2000
3000
4000
Age (ka)

Figure 2

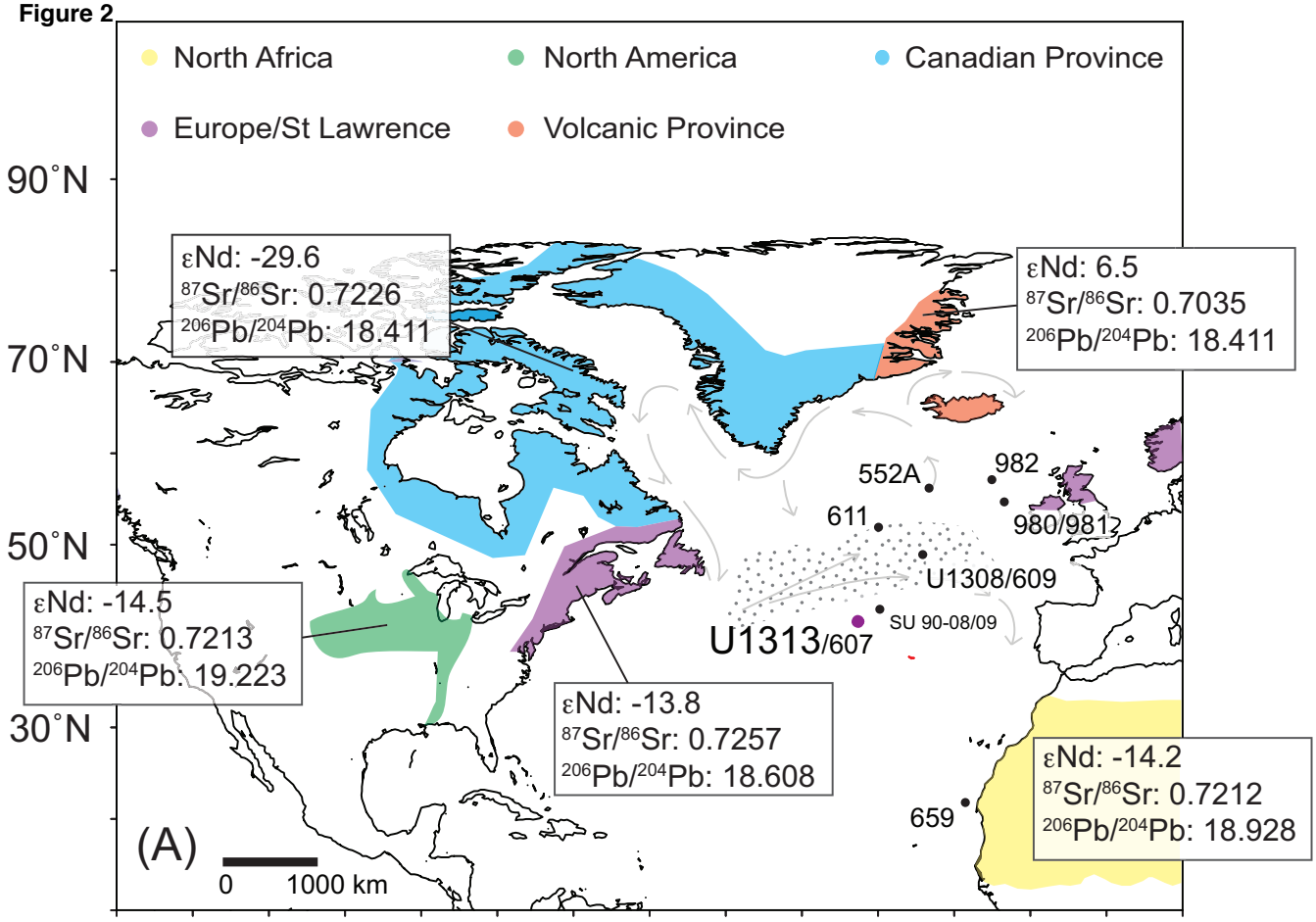
North Africa
North America
Canadian Province
Europe/St Lawrence
Volcanic Province
90˚N
70˚N
50˚N
30˚N
εNd: -29.6
87Sr/86Sr: 0.7226
206Pb/204Pb: 18.411
εNd: 6.5
87Sr/86Sr: 0.7035
206Pb/204Pb: 18.411
552A
982
611
980/981
U1308/609
SU 90-08/09
U1313/607
εNd: -14.5
87Sr/86Sr: 0.7213
206Pb/204Pb: 19.223
εNd: -13.8
87Sr/86Sr: 0.7257
206Pb/204Pb: 18.608
εNd: -14.2
87Sr/86Sr: 0.7212
206Pb/204Pb: 18.928
659
(A)
0
1000 km

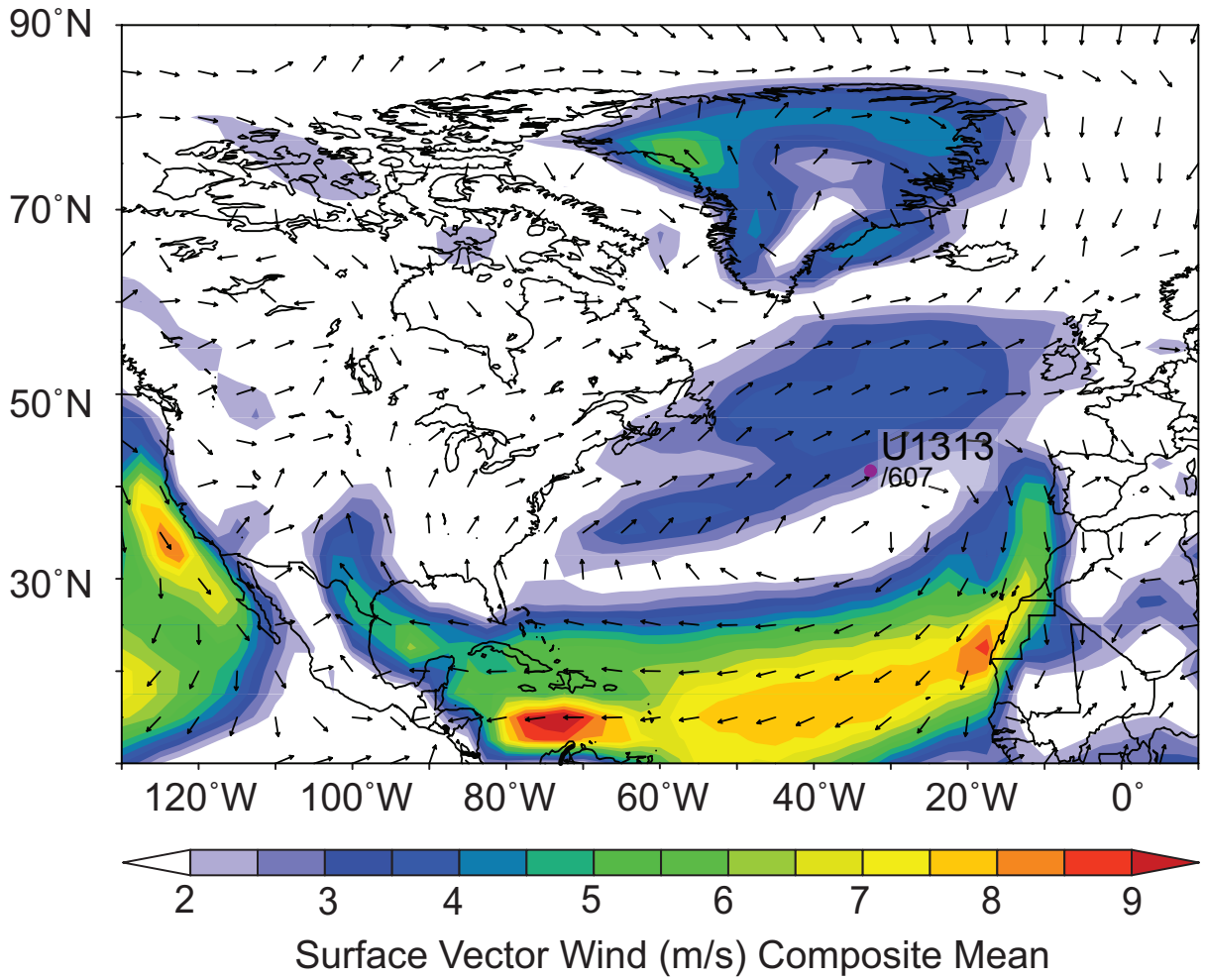
90˚N
70˚N
50˚N
30˚N
U1313
/607
120˚W
100˚W
80˚W
60˚W
40˚W
20˚W
0˚
2
3
4
5
6
7
8
9
Surface Vector Wind (m/s) Composite Mean

Figure 3

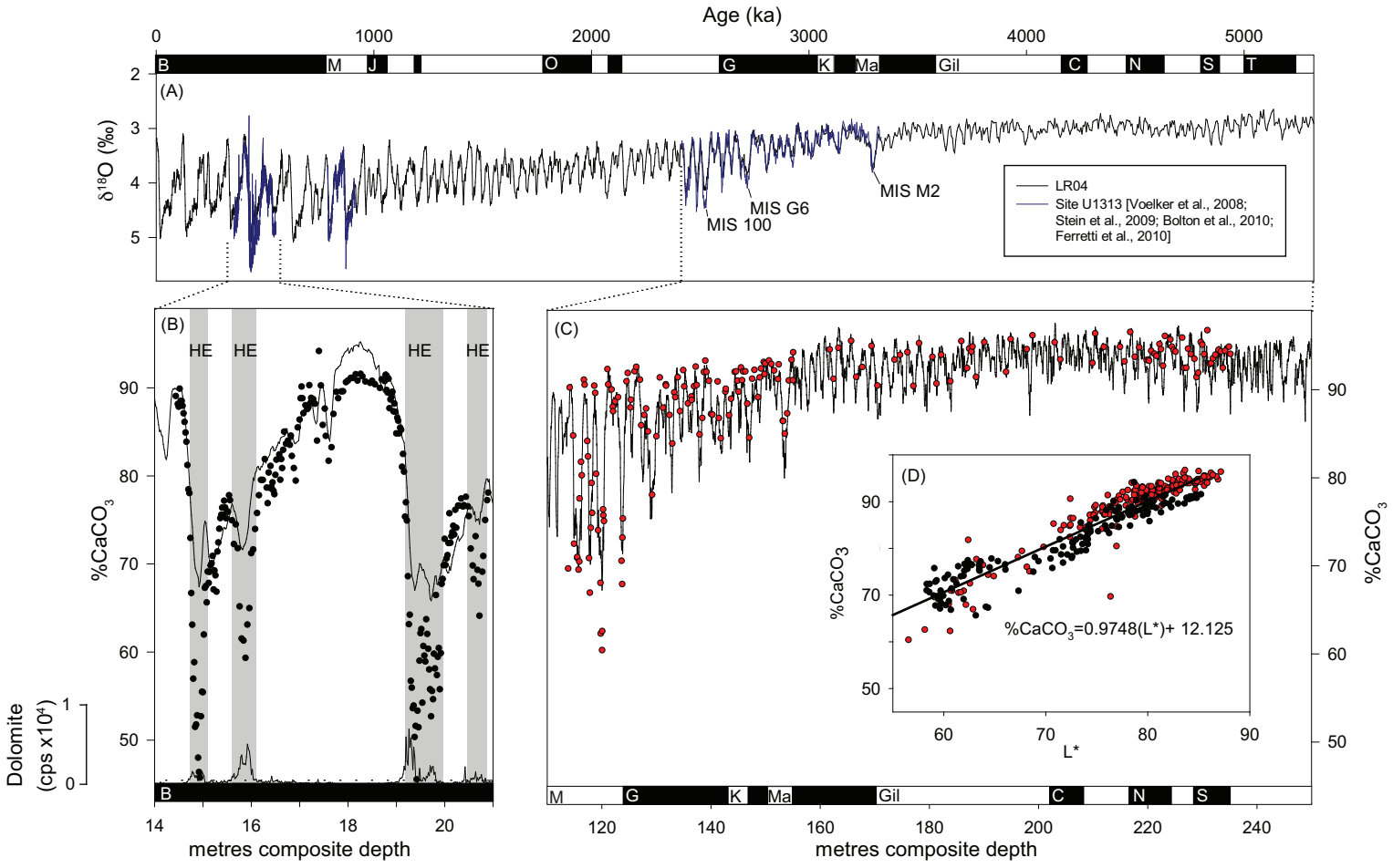
Age (ka)
0
1000
2000
3000
4000
5000
B
M
J
O
G
K
Ma
Gil
C
N
S
T
(A)
δ18O (‰)
MIS 100
MIS G6
MIS M2
LR04
Site U1313 [Voelker et al., 2008; Stein et al., 2009; Bolton et al., 2010; Ferretti et al., 2010]
(B)
HE
HE
HE
HE
%CaCO3
Dolomite (cps x10^4)
metres composite depth
(C)
(D)
%CaCO3=0.9748(L*)+ 12.125
L*
metres composite depth

Figure 5

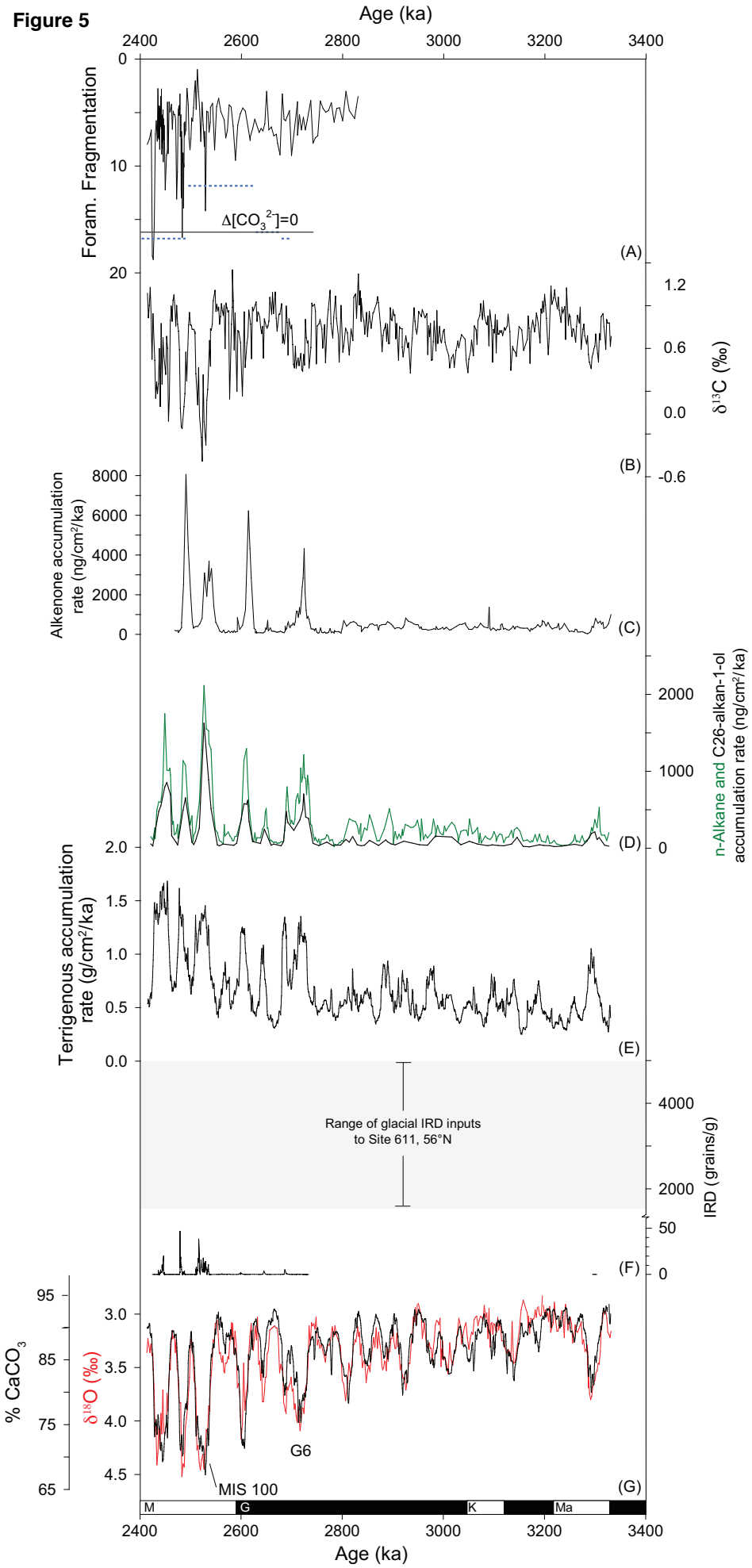
Age (ka)
2400
2600
2800
3000
3200
3400
Foram. Fragmentation
0
10
20
Δ[CO3 2-]=0
(A)
1.2
0.6
0.0
-0.6
δ13C (‰)
(B)
Alkenone accumulation rate (ng/cm2/ka)
8000
6000
4000
2000
0
(C)
2000
1000
0
n-Alkane and C26-alkan-1-ol accumulation rate (ng/cm2/ka)
(D)
Terrigenous accumulation rate (g/cm2/ka)
2.0
1.5
1.0
0.5
0.0
(E)
Range of glacial IRD inputs to Site 611, 56°N
4000
2000
IRD (grains/g)
50
0
(F)
% CaCO3
95
85
75
65
δ18O (‰)
3.0
3.5
4.0
4.5
G6
MIS 100
(G)
M
G
K
Ma
2400
2600
2800
3000
3200
3400
Age (ka)

Figure 4

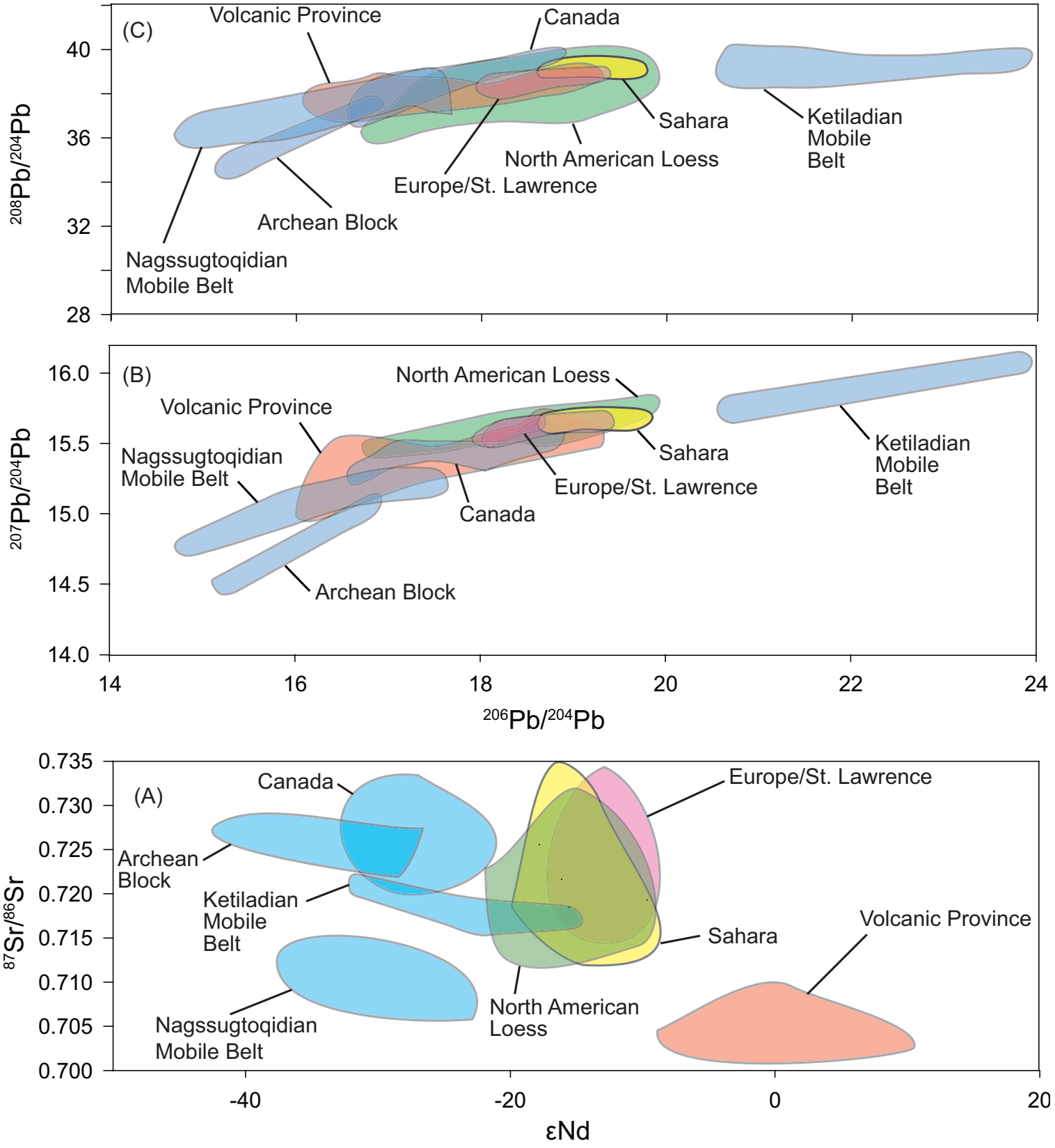
(C)
Volcanic Province
Canada
Sahara
Ketiladian
Mobile
Belt
North American Loess
Europe/St. Lawrence
Archean Block
Nagssugtoqidian
Mobile Belt
208Pb/204Pb
40
36
32
28
(B)
North American Loess
Volcanic Province
Sahara
Ketiladian
Mobile
Belt
Nagssugtoqidian
Mobile Belt
Europe/St. Lawrence
Canada
Archean Block
207Pb/204Pb
16.0
15.5
15.0
14.5
14.0
14
16
18
20
22
24
206Pb/204Pb
(A)
Canada
Europe/St. Lawrence
Archean
Block
Ketiladian
Mobile
Belt
Sahara
Volcanic Province
North American
Loess
Nagssugtoqidian
Mobile Belt
87Sr/86Sr
0.735
0.730
0.725
0.720
0.715
0.710
0.705
0.700
-40
-20
0
20
εNd

Figure 6

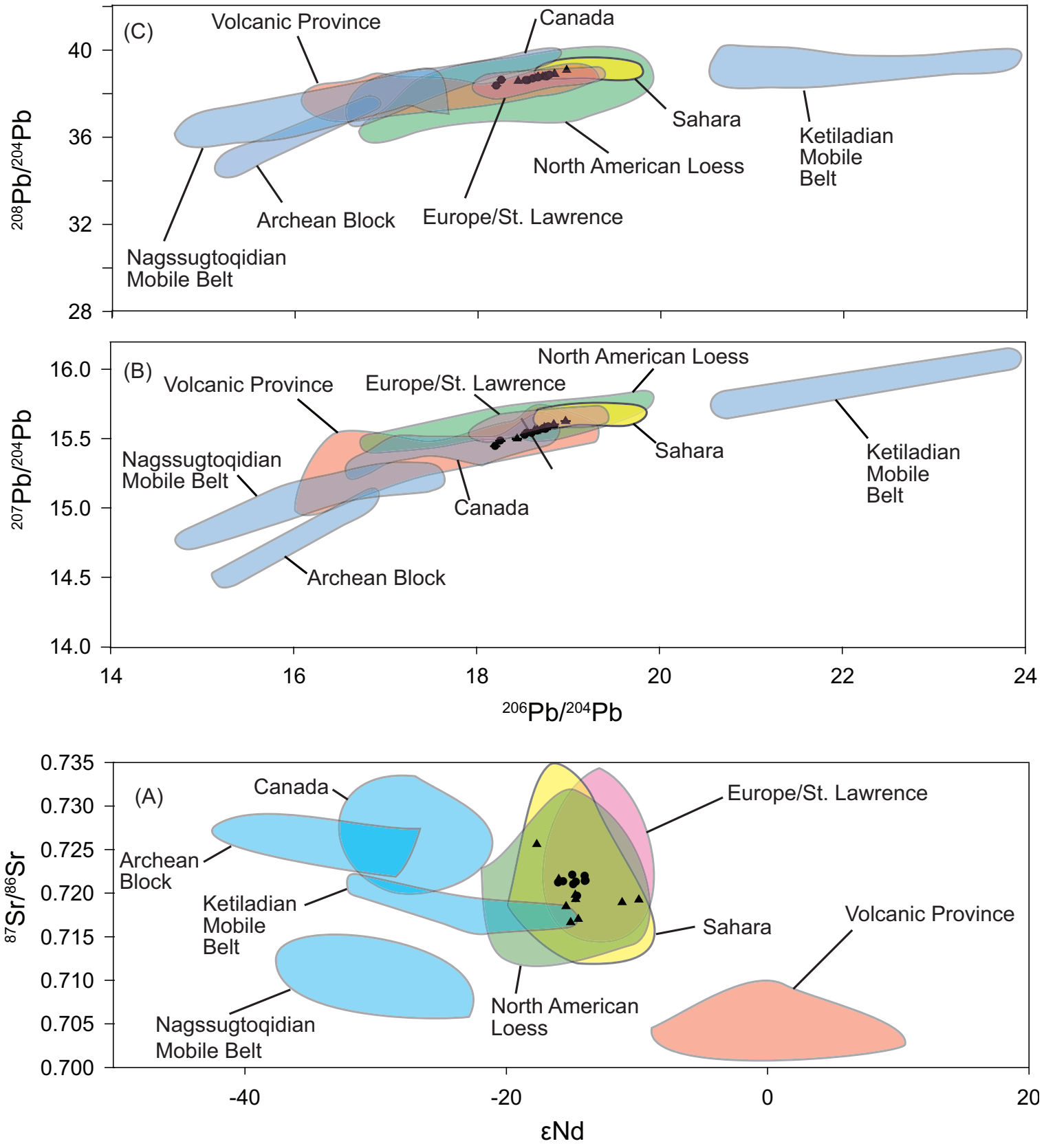
(C)
Volcanic Province
Canada
Sahara
Ketiladian
Mobile
Belt
North American Loess
Archean Block
Europe/St. Lawrence
Nagssugtoqidian
Mobile Belt
208Pb/204Pb
40
36
32
28
(B)
North American Loess
Volcanic Province
Europe/St. Lawrence
Sahara
Ketiladian
Mobile
Belt
Nagssugtoqidian
Mobile Belt
Canada
Archean Block
207Pb/204Pb
16.0
15.5
15.0
14.5
14.0
14
16
18
20
22
24
206Pb/204Pb
(A)
Canada
Europe/St. Lawrence
Archean
Block
Ketiladian
Mobile
Belt
Sahara
Volcanic Province
North American
Loess
Nagssugtoqidian
Mobile Belt
87Sr/86Sr
0.735
0.730
0.725
0.720
0.715
0.710
0.705
0.700
-40
-20
0
20
εNd

Figure 7

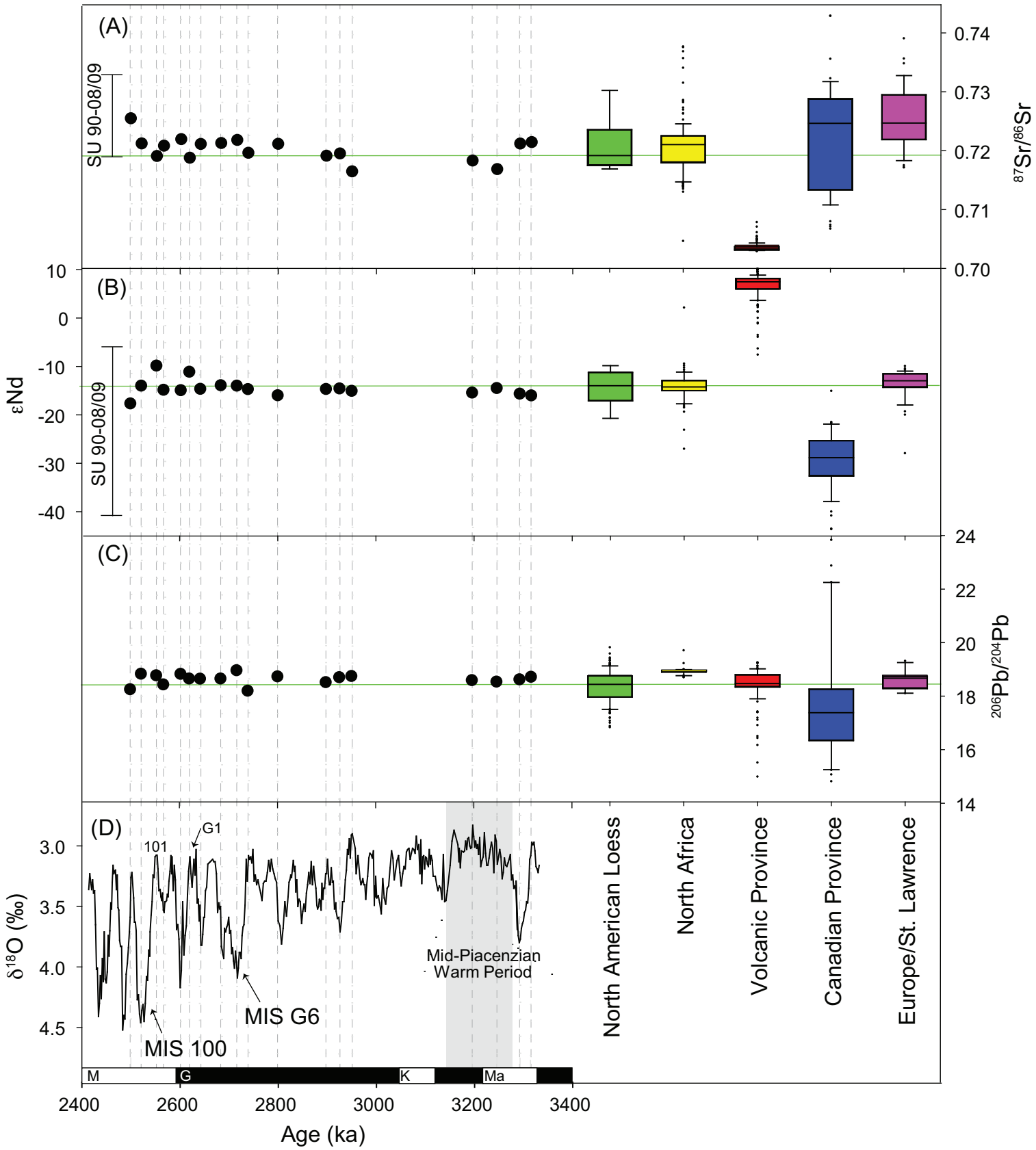
(A)
SU 90-08/09
0.74
0.73
0.72
0.71
0.70
$^{87}Sr/^{86}Sr$
(B)
SU 90-08/09
10
0
-10
-20
-30
-40
εNd
(C)
24
22
20
18
16
14
$^{206}Pb/^{204}Pb$
(D)
101
G1
MIS 100
MIS G6
Mid-Piacenzian
Warm Period
3.0
3.5
4.0
4.5
$\delta^{18}O$ (‰)
M
G
K
Ma
2400
2600
2800
3000
3200
3400
Age (ka)
North American Loess
North Africa
Volcanic Province
Canadian Province
Europe/St. Lawrence

Figure 8

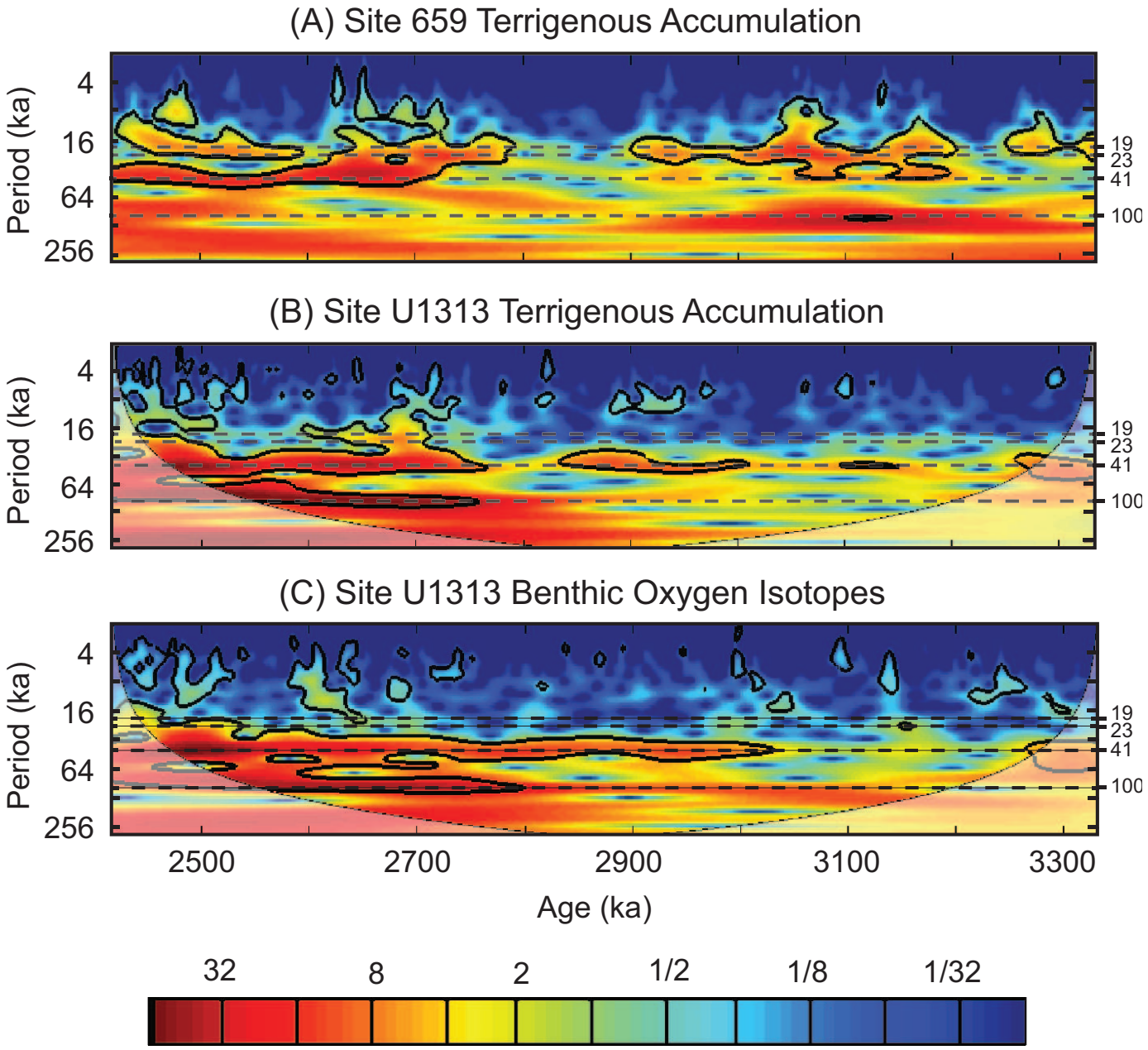
(A) Site 659 Terrigenous Accumulation
(B) Site U1313 Terrigenous Accumulation
(C) Site U1313 Benthic Oxygen Isotopes
Period (ka)
4
16
64
256
19
23
41
100
2500
2700
2900
3100
3300
Age (ka)
32
8
2
1/2
1/8
1/32

Figure 9

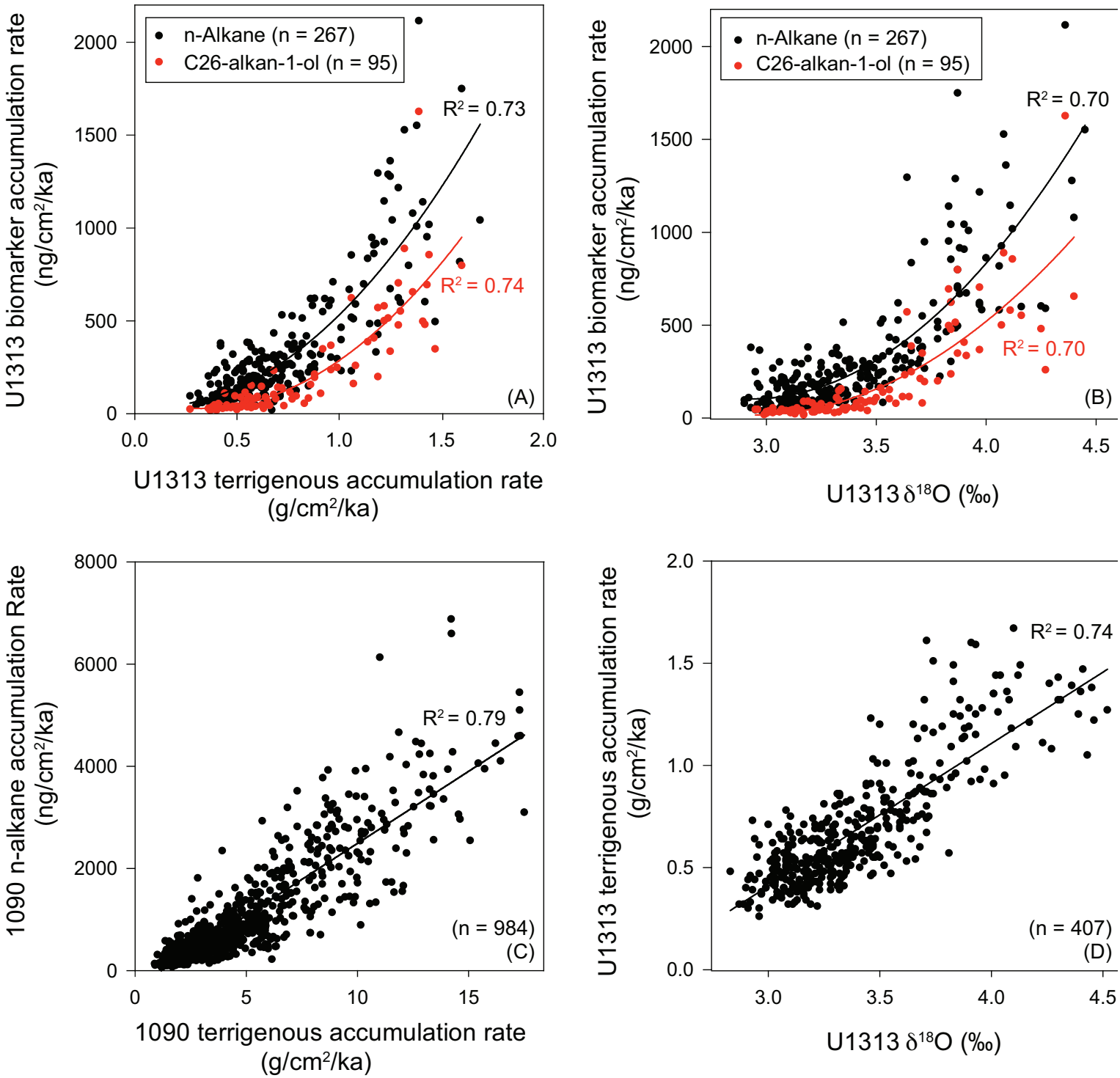
n-Alkane (n = 267)
C26-alkan-1-ol (n = 95)
R² = 0.73
R² = 0.74
(A)
U1313 biomarker accumulation rate (ng/cm²/ka)
U1313 terrigenous accumulation rate (g/cm²/ka)
R² = 0.70
R² = 0.70
(B)
U1313 δ¹⁸O (‰)
1090 n-alkane accumulation Rate (ng/cm²/ka)
R² = 0.79
(n = 984)
(C)
1090 terrigenous accumulation rate (g/cm²/ka)
U1313 terrigenous accumulation rate (g/cm²/ka)
R² = 0.74
(n = 407)
(D)
U1313 δ¹⁸O (‰)

Figure 10

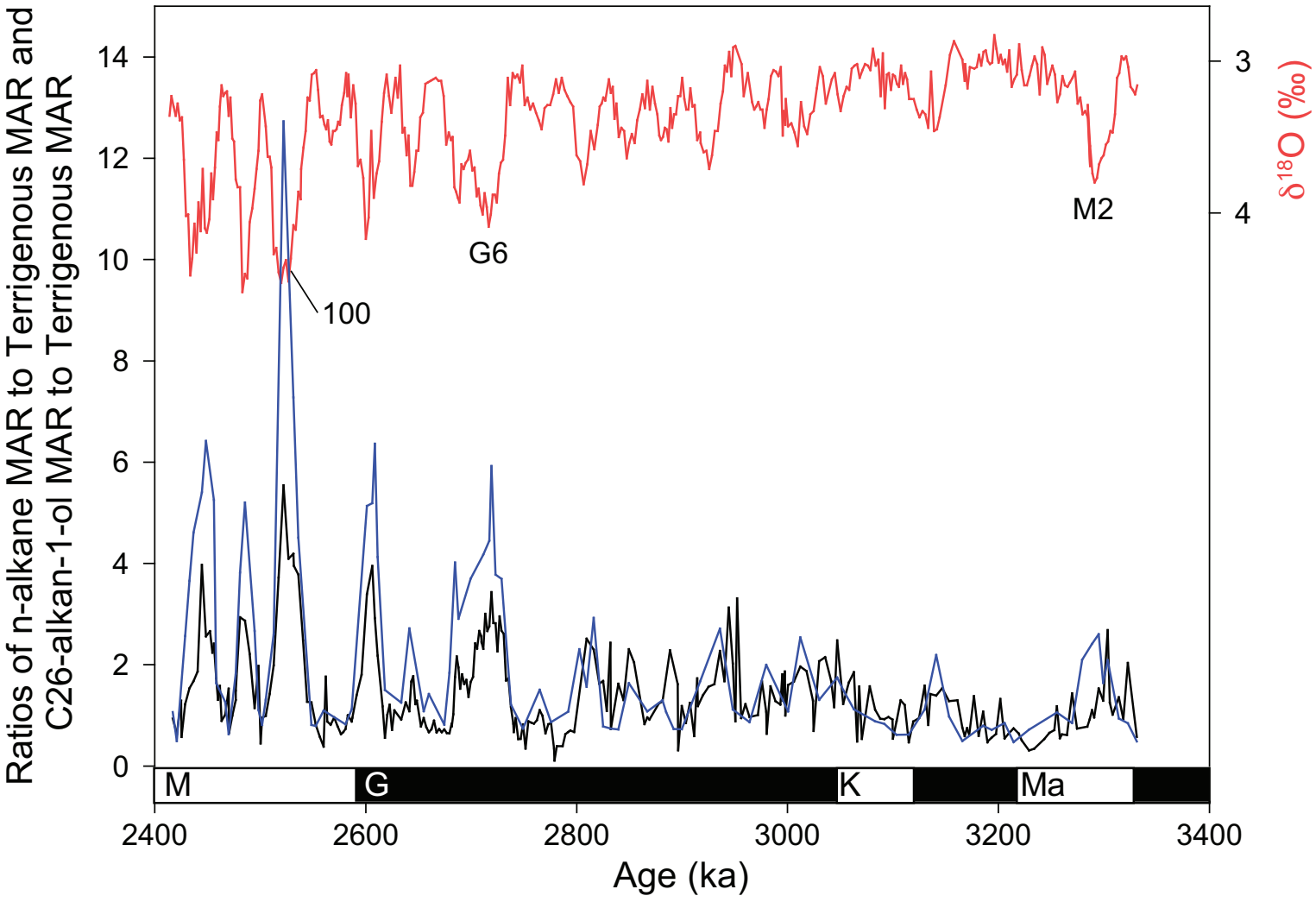
Ratios of n-alkane MAR to Terrigenous MAR and
C26-alkan-1-ol MAR to Terrigenous MAR
δ18O (‰)
Age (ka)
100
G6
M2
M
G
K
Ma
0
2
4
6
8
10
12
14
3
4
2400
2600
2800
3000
3200
3400

Figure 11

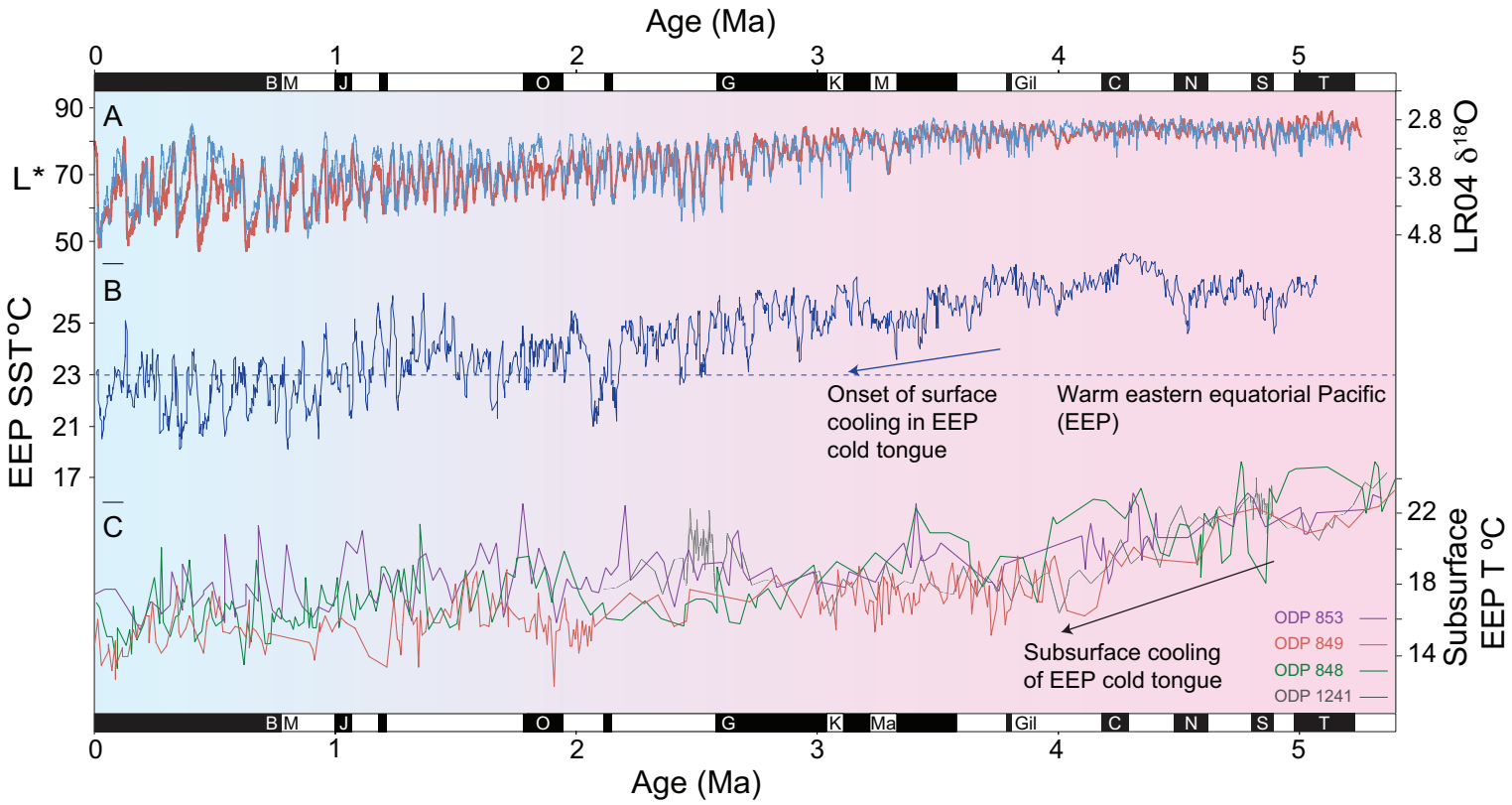
Age (Ma)
0
1
2
3
4
5
B M J O G K M Gil C N S T
A
B
C
L*
90
70
50
25
23
21
17
EEP SST°C
LR04 δ18O
2.8
3.8
4.8
Onset of surface cooling in EEP cold tongue
Warm eastern equatorial Pacific (EEP)
Subsurface cooling of EEP cold tongue
ODP 853
ODP 849
ODP 848
ODP 1241
22
18
14
Subsurface EEP T °C
B M J O G K Ma Gil C N S T
Age (Ma)

Supplementary Data

Click here to download Supplementary Data: Lang et al. supplementary information.pdf

'Equation File' for editorial office

Click here to download Supplementary Data: Epsilon Nd equation.docx